

1 **Urban-rural patterns and driving factors of particulate 2 matter pollution decrease in eastern china**

3 Zhihao Song^{1, 2}, Bin Chen^{1, 2*}

4 ¹ College of Atmospheric Sciences, Lanzhou University, Lanzhou 730000, China

5 ² Institute of Meteorological Artificial Intelligence Research, Lanzhou University, Lanzhou 730000, China

6 *Correspondence to:* Bin Chen (chenbin@lzu.edu.cn)

7 **Abstract.** Urban-rural patterns of particulate matter (PM) pollution reduction in China remain poorly
8 understood. Using an interpretable end-to-end machine learning model framework from original satellite
9 data, we identified changes in urban and rural PM pollution and the underlying drivers. During the period
10 2015-2023, the average decrease rates of PM₁₀ and PM_{2.5} in eastern China were $-4.02 \pm 1.29 \mu\text{g}/\text{m}^3/\text{yr}$ and
11 $-2.41 \pm 0.91 \mu\text{g}/\text{m}^3/\text{yr}$, respectively. The rate of decrease in urban areas was higher than that in rural areas,
12 which played a dominant role in PM reduction. Significant reductions in PM concentrations were
13 observed in urban core areas, suburbs, towns and regions with high agricultural pressure. The
14 interpretability analysis showed that temperature and interannual variability were the main drivers of PM
15 pollution reduction. However, only interannual variability showed a significant decreasing trend in its
16 effect on PM pollution, while other driving factors showed periodic variations. Furthermore, there were
17 differences in the drivers of PM reduction between urban and rural areas, particularly with interannual
18 variability in particular contributing to PM pollution reduction in urban areas, but having a lesser impact
19 in most rural areas. This study reveals the urban-rural patterns of PM pollution reduction in eastern China,
20 and highlights the need for differentiated air pollution control strategies in urban and rural areas.

21 **1 Introduction**

22 Air pollution caused by PM_{2.5} and PM₁₀ (airborne particulate matter with diameters less than 2.5 μm
23 and 10 μm , respectively) has adversely affected China's atmospheric environment (Huang et al., 2014a;
24 Zhang et al., 2012). PM pollution is now considered the greatest environmental risk factor for global
25 human health (Apte et al., 2015), as exposure to PM can trigger various respiratory and cardiovascular
26 diseases (Burnett Richard et al., 2014; West et al., 2016; Cohen et al., 2017). The indirect health risks
27 associated with PM exposure (Yin et al., 2020) contribute to millions of premature deaths annually in

28 China (Burnett et al., 2018). To mitigate the escalating risks of particulate matter exposure and reduce
29 the public health burden, the Chinese government introduced the "Air Pollution Prevention and Control
30 Action Plan" in 2013 (State Council of the People's Republic of China, 2013). This initiative aims to
31 implement policies to improve energy efficiency, reduce energy-related pollution, and curb
32 anthropogenic emissions to control particulate matter pollution in the atmosphere (State Council of the
33 People's Republic of China, 2014). As a result of this initiative, China's atmospheric particulate matter
34 pollution has improved significantly (Cheng et al., 2021). Between 2013 and 2017, the annual average
35 concentration of $PM_{2.5}$ decreased by 28-40% (Zheng et al., 2018; Ministry of Ecology and Environment
36 of the People's Republic of China, 2017), and the population-weighted national annual average
37 concentration of $PM_{2.5}$ decreased by 32% (Xue et al., 2019). Data from the National Air Quality
38 Monitoring Network show that between 2013 and 2020, the annual average $PM_{2.5}$ concentration in urban
39 areas of China decreased from $72 \mu\text{g}/\text{m}^3$ to $33 \mu\text{g}/\text{m}^3$ (Song et al., 2023). As a result, the Clean Air Action
40 has achieved remarkable results in reducing PM pollution (Zhang et al., 2019b).

41 It is widely accepted that improvements in air quality can be attributed to both reductions in
42 anthropogenic emissions (Geng et al., 2019; Zheng et al., 2023; Zhao et al., 2018) and changes in
43 meteorological conditions (An et al., 2019; Cao and Yin, 2020; Chen et al., 2020a). To assess the driving
44 factors behind changes in PM concentration trends, it is essential to distinguish between anthropogenic
45 emissions and meteorological factors (Zhong et al., 2018). Zhong et al. (2021) found that $PM_{2.5}$
46 concentrations decreased by 44% from 2013 to 2019, and by 34% when the influence of meteorological
47 conditions was excluded, thus demonstrating the effectiveness of emission reduction measures. Qiu et al.
48 (2022) used the GEOS-Chem chemical transport model to simulate the impact of anthropogenic
49 emissions on PM pollution trends and provided recommendations for attributing PM pollution trends to
50 emission changes. Vu et al. (2019) used machine learning to assess the impact of air quality trends in
51 Beijing and found that $PM_{2.5}$ and PM_{10} concentrations decreased by 34% and 24%, respectively, after
52 excluding meteorological influences, attributing the decrease to reduced coal burning. Zhai et al. (2019)
53 used a stepwise multiple linear regression (MLR) model to quantify $PM_{2.5}$ trends in China between 2013
54 and 2018, and found that meteorological conditions contributed about 12%. However, Xiao et al. (2021)
55 used statistical methods to separate the contributions of emissions and meteorology to long-term $PM_{2.5}$
56 trends in East China, and found that meteorological contributions were even higher in certain years.

57 Overall, distinguishing the contributions of anthropogenic emissions and meteorological changes to PM
58 pollution is crucial to improve understanding of pollution processes and to inform pollution control
59 policies and future air quality predictions.

60 However, the urban-rural patterns of PM pollution improvement remain poorly understood in
61 existing research (Chen et al., 2020b). Many studies on PM pollution either focus on highly polluted
62 regions (such as the Beijing-Tianjin-Hebei region) (Chen et al., 2019b; Chen et al., 2019c), or on
63 developed regions with a high concentration of large cities (such as the Yangtze River Delta and the
64 Pearl River Delta) (Gui et al., 2019; He et al., 2017). This focus is mainly due to the high concentrations
65 of air pollutants in developed cities (Sicard et al., 2023), where PM pollution poses a significant public
66 health threat to densely populated urban areas (Brauer et al., 2016; Southerland et al., 2022). Although
67 PM pollution in urban areas highlights the importance of environmental governance, rural areas, with
68 different consumption habits and living conditions (e.g., solid fuel burning in households) (Li et al.,
69 2014)), may experience air pollution that differs from urban areas (Wang et al., 2024a). In certain seasons
70 and regions, PM exposure factors in rural areas are generally higher than those in urban areas, with
71 exposure levels reaching up to 70% (Wang et al., 2024b). Therefore, the contribution of these regions to
72 PM pollution improvement may differ (Li et al., 2024b). Without targeted assessments, perceptions of
73 the relative importance of urban and rural areas in China's air pollution control efforts may be distorted,
74 hindering the development of appropriate environmental policies and the promotion of green
75 development in urban and rural construction (Yang et al., 2024).

76 Currently, many studies have used machine learning models to obtain particulate matter
77 concentration products and apply them to pollution assessment (Chen et al., 2019a; Huang et al., 2021).
78 Among these, extreme tree models and data from the Himawari-8 satellite have demonstrated outstanding
79 performance (Wei et al., 2021b; Wei et al., 2021a; Wei et al., 2021c). In particular, the extreme tree
80 model demonstrates its unique advantages, including greater randomness and interference resistance, and
81 outperforms other similar models in terms of performance (Wei et al., 2023). This study advances the
82 understanding of the current status and driving factors of urban-rural PM pollution improvement using
83 interpretable machine learning methods. First, by integrating Himawari-8/9 satellite top-of-atmosphere
84 reflectance (TOAR) data, meteorological data, and geographic information, we use a multiple-output
85 extreme trees (MOET) model to capture the spatiotemporal distribution of PM (including PM₁₀ and PM_{2.5})

86 across China and assess the patterns of PM pollution improvement. We then use various machine learning
87 interpretability techniques, such as relative importance, tree interpreters, and SHAP values, to quantify
88 the contributions of anthropogenic emissions and meteorological changes to PM pollution improvement.
89 To investigate potential differences in the results between urban and rural areas, we use land use data to
90 distinguish urban from rural regions in eastern China. This study aims to address the following three
91 questions: (1) What are the spatio-temporal patterns of PM pollution improvement in urban and rural
92 areas of China? (2) What are the main driving factors behind the differences in PM pollution
93 improvement between urban and rural areas? (3) What are the specific contributions of each driving
94 factor to PM pollution improvement? Answering these questions is crucial for a comprehensive
95 understanding of the dynamics of urban and rural atmospheric particulate pollution control in China.

96 **2 Data and Methods**

97 **2.1 Satellite TOAR data and ground-based PM observations**

98 Previous studies have shown that satellite-observed top-of-atmosphere reflectance (TOAR) data
99 can be used to estimate near-surface air pollutants (Chen et al., 2024a; Yang et al., 2023; Song et al.,
100 2024). In particular, the TOAR data from the Himawari-8 satellite have demonstrated excellent
101 performance in pollutant estimation (Hu et al., 2022; Liu et al., 2019). The Advanced Himawari Imager
102 (AHI) on board the Himawari-8/9 satellite is an advanced passive observation instrument with 16
103 observation channels, providing a spatiotemporal resolution of up to 10 minutes and 0.5 km (Bessho et
104 al., 2016). Based on the sensitivity of the AHI sensor (Yoshida et al., 2018), three visible channels (0.46
105 μm , 0.51 μm , and 0.64 μm) and two near-infrared channels (0.86 μm and 2.3 μm) were used in this study.

106 In addition, four angles related to aerosol inversion results: SAA (satellite azimuth angle), SAZ (satellite
107 zenith angle), SOA (solar azimuth angle), and SOZ (solar zenith angle) were also included in the study.
108 TOAR data from the AHI imager were obtained from the Himawari Monitor P-Tree System data
109 download website of the Japan Meteorological Agency (<https://www.eorc.jaxa.jp/ptree/index.html>). The
110 time range for Himawari-8 data is from September 1, 2015, to September 30, 2022, while the time range
111 for Himawari-9 data is from October 1, 2022, to August 31, 2023.

112 The ground-based PM data were provided by the China National Environmental Monitoring Center
113 (CNEMC) (<http://www.cnemc.cn>) and were calibrated and quality controlled according to the Chinese

114 National Standard GB 3095-2012 (Ministry of Ecology and Environment of the People's Republic of
115 China, 2012). In this study, hourly mean PM_{10} and $PM_{2.5}$ data were collected from approximately 1,400
116 stations in eastern China (102-136°E, 16-56°N) for the period from 1 September 2015 to 31 August 2023.
117 Observations with $PM_{2.5}$ concentrations above 600 $\mu\text{g}/\text{m}^3$ or PM_{10} concentrations above 1,000 $\mu\text{g}/\text{m}^3$, as
118 well as those with concentrations below 1 $\mu\text{g}/\text{m}^3$, were excluded (Shi et al., 2024).

119 **2.2 Meteorological data and geographic information data**

120 Studies assessing the impact of meteorological factors on PM pollution have identified temperature,
121 humidity, and wind as the main variables influencing $PM_{2.5}$ concentrations, with their effects
122 significantly outweighing those of other factors. Among these, temperature has the most significant
123 and stable influence (Chen et al., 2018b). In this study, meteorological data were obtained from
124 the ERA-5 reanalysis dataset provided by the European Centre for Medium-Range Weather Forecasts
125 (<https://cds.climate.copernicus.eu/cdsapp#!/dataset/>). The dataset includes boundary layer height
126 (BLH), relative humidity (RH), surface pressure (SP), 2-metre air temperature (T2M), wind direction
127 (WD), wind speed (WS), and net solar radiation at the surface (NSR), with spatial resolutions of
128 $0.1^\circ \times 0.1^\circ$ or $0.25^\circ \times 0.25^\circ$ (Hersbach et al., 2020). Geographic information can also influence
129 pollutant concentrations to some extent due to variations in meteorological conditions (Chen
130 et al., 2018a; Chen et al., 2021). The geographic information data used in this study include elevation
131 (HEIGHT), land cover type (LUCC), and population density (RK). HEIGHT is derived from
132 SRTM-3 elevation data, with a spatial resolution of 90 meters and a temporal resolution of 1 year.
133 The download URL is <https://doi.org/10.5067/MEaSUREs/SRTM/SRTMGL3.003>. LUCC is sourced
134 from the dataset (MCD12Q1), with a spatial resolution of 500 meters and a temporal resolution
135 of 1 year. The download URL is <https://doi.org/10.5067/MODIS/MCD12Q1.006>, used to describe
136 land surface types and land use conditions. RK is derived from the 2015 United Nations adjusted
137 population density data, with a spatial resolution of $0.1^\circ \times 0.1^\circ$ and a temporal resolution of 1 year,
138 available at <https://doi.org/10.7927/H4PN93PB>. It is provided by the Social and Economic Data
139 and Applications Center (SEDAC) of the National Aeronautics and Space Administration (NASA
140 A).

141 **2.3 Data integration and development of the Multiple-Output Extreme Trees Model**

142 The resolution of the meteorological and geographic information data was adjusted to $0.05^\circ \times 0.05^\circ$
143 using bilinear interpolation. All data were then matched with station data according to the $0.05^\circ \times 0.05^\circ$
144 grid of the Himawari-8 satellite. The specific matching method is described in detail in Chen et al. (2022c)
145 and Song et al. (2022b).

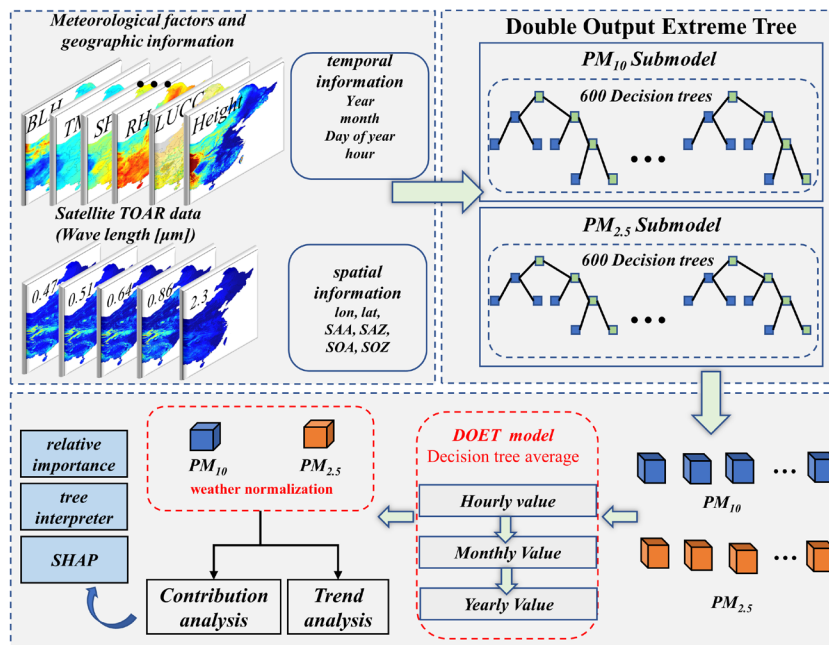
146 The DOET model is developed on the basis of the Extreme Trees (ET) model (Geurts et al., 2006),
147 which is capable of simultaneously handle multi-target variable output tasks. The ET model is similar to
148 the Random Forest (RF) model, both of which consist of multiple decision trees. However, whereas the
149 RF model randomly samples data with replacement, the ET model uses all available samples. After
150 determining the samples and features, the ET model constructs decision trees based on optimal partition
151 attributes. This process is repeated until a sufficient number of decision trees have been constructed to
152 form the ET model. Finally, the average regression results of all decision trees in the ET are used as the
153 final output. Several studies have confirmed that the ET model has excellent fitting performance (Qin et
154 al., 2020; Zhang et al., 2022a; Chen et al., 2022a).

155 In this study, three model parameters were optimized: the number of trees (n_estimators), the
156 maximum depth of the model (max_depth), and the minimum number of samples required to split a node
157 (min_samples_split). After balancing the accuracy and efficiency of the model, these parameters were
158 set to 70, 100, and 5, respectively. The model, which uses satellite observations, meteorological data,
159 and geographical information to estimate near-surface PM concentrations, can be expressed as:

$$160 (PM_{10}, PM_{2.5}) = f \left(TOAR_{1,2,3,4,6}, BLH, RH, SP, T2M, WD, WS, NSR, Height, LUCC, RK, \right) \quad (1)$$

161 Here, f represents the DOET model, and $TOAR_{1,2,3,4,6}$ denotes the radiance values of the three
162 visible channels (0.46 μm , 0.51 μm , and 0.64 μm) and the two near-infrared channels (0.86 μm and 2.3
163 μm). $BLH, RH, SP, T2M, WD, WS$ and NSR are meteorological variables, while $Height, LUCC$ and
164 RK represent geographical information. The variables lon (Longitude), lat (Latitude), SAA, SAZ, SOA
165 and SOZ representing spatial information. The variables $year$, mon (month), doy (day of the year), and
166 $hour$ are temporal information reflecting the influence of anthropogenic emissions on PM pollution (Wei
167 et al., 2020). Time variables (year, month) effectively characterize cyclical patterns and long-term trends
168 in human activity, serving as reliable proxy indicators in pollution analysis (Song et al., 2023). Monthly

169 cycles directly reflect seasonal rhythms: winter heating spikes PM2.5 and SO₂ levels (Liu et al., 2017),
 170 agricultural phases amplify ammonia emissions (Ma et al., 2025), and transportation peaks during
 171 holidays elevate NO₂ concentrations (Hua et al., 2021). Annual trends capture industrial evolution and
 172 policy impacts, such as the PM2.5 reduction after implementing the "Air Pollution Prevention Action
 173 Plan" (Geng et al., 2024; Geng et al., 2021). As standardized, quantifiable metrics, time variables
 174 circumvent data limitations for complex activities (e.g., energy consumption, economic behaviors, urban
 175 sprawl), enable cross-regional comparisons without normalization, and reveal pollution responses to
 176 socioeconomic rhythms and policy efficacy (Dai et al., 2021; Shi et al., 2021). Specifically, year and
 177 month (mon) are used to represent the interannual and intra-annual variations in anthropogenic emissions,
 178 respectively (Zhang et al., 2019a; Park et al., 2019). The estimation workflow is illustrated in Figure 1.
 179 The specific estimation process of the DOET model is as follows: firstly, meteorological factors,
 180 geographic information, and satellite TOAR data are input into the DOET model and matched with PM
 181 observation data. Then, the DOET model fits the PM observation data with the input variables to obtain
 182 two ET estimation models (PM₁₀ and PM_{2.5}). Finally, the two ET models are integrated to obtain the
 183 DOET model, and the estimation results of PM₁₀ and PM_{2.5} are output simultaneously to save
 184 computation time. Finally, the obtained PM₁₀ and PM_{2.5} data are subjected to further analysis.
 185 Additionally, we performed weather normalization on the PM data to mitigate the impact of
 186 meteorological events (Grange and Carslaw, 2019).



187
 188 **Figure 1. Workflow of PM data estimation and pollution driving factors assessment.**

189 Model performance was evaluated using 10-fold cross-validation (Rodriguez et al., 2010),
190 incorporating sample-based, space-based, and time-based validation methods (Wei et al., 2019).
191 Evaluation metrics used included the coefficient of determination (R^2), root mean square error (RMSE),
192 and mean absolute error (MAE) for both PM_{10} and $PM_{2.5}$ (Chen et al., 2023).

193
$$R^2 = 1 - \frac{ss_{res}}{ss_{tot}} \quad (2)$$

194
$$MAE = \frac{1}{n} \sum_{i=1}^n |\hat{y}_i - y_i| \quad (3)$$

195
$$RMSE = \sqrt{\frac{1}{n} \sum_{i=1}^n (\hat{y}_i - y_i)^2} \quad (4)$$

196 In Equation (2), ss_{res} represents the error between the estimated value of the model and the
197 average value of the observed values of PM_{10} and $PM_{2.5}$, ss_{tot} represents the error between the observed
198 values of PM_{10} and $PM_{2.5}$ and the average value of the observed values of PM_{10} and $PM_{2.5}$ from CNEMC.
199 In Equation (3-5), \hat{y}_i represents the PM_{10} and $PM_{2.5}$ estimated value of the DOET model, y_i represents
200 the observed value of PM_{10} and $PM_{2.5}$ from CNEMC.

201 **2.4 Machine learning interpretability variables**

202 To investigate the influence of potential driving factors on PM pollution improvement in eastern
203 China, we employed relative importance (Berner et al., 2020), tree interpreter (Wang et al., 2022b), and
204 SHapley Additive exPlanations (SHAP) (Lundberg and Lee, 2017) to distinguish the contributions of
205 meteorological changes and anthropogenic emissions to PM pollution improvement. Relative importance
206 was assessed using the permutation importance value of the DOET model, defined as the average
207 reduction in model accuracy when a single feature value is randomly shuffled (Yang et al., 2022).

208 The permutation importance of each variable was calculated using the "permutation_importance"
209 library in Python. To reduce uncertainty, the training process was repeated 20 times for each grid point
210 to obtain robust estimates of relative importance (Qu et al., 2023). The tree interpreter was applied using
211 the 'tree_interp_functions' library in Python, which is designed for predictions based on decision tree
212 ensemble models and facilitates the decomposition of each prediction into bias and feature contribution
213 components. The detailed calculation method and code for the tree interpreter can be obtained from the
214 following URL:<https://github.com/andosa/treeinterpreter/tree/master>.

215 SHAP values are based on Shapley value theory, which explains model predictions by calculating

216 the relative contribution of each feature to the output (He et al., 2024). These values reflect not only the
217 influence of features on individual samples but also indicate the positive and negative contributions of
218 these influences. SHAP explanations can be applied to any machine learning model, including neural
219 networks and ensemble models, and provide comprehensive and accurate interpretability results. Thus,
220 the SHAP method provides superior explanations for both local and global model effects (Liu et al., 2023;
221 Hou et al., 2022). In Python, “tree_SHAP” is specifically tailored for decision tree-based machine
222 learning models, such as the Extreme Tree model, to provide greater accuracy and faster computation.

223 The interpretability variables described above were applied to the monthly averaged PM₁₀ and PM_{2.5}
224 datasets generated by the DOET model.

225 **2.5 Land cover type classification**

226 Zhang et al. (2022b) proposed a method to differentiate urban and rural areas based on the gradient
227 of human land use pressure. In this study, the MCD12Q1 land cover map, with a spatial resolution of 500
228 meters was used. For grids measuring 5×5 km, urban and rural classifications were determined by the
229 coverage of specific land cover categories (e.g., urban land and cropland), which reflect the transition
230 from urban to rural areas and correspond to different levels of human activity. As shown in Table 1 and
231 Figure S1, urban areas in this study include both urban core areas and suburban regions, while rural areas
232 are categorized into six types: towns, high agricultural pressure areas, low agricultural pressure areas,
233 forests and grasslands.

234 **Table 1. Definitions of urban and rural land cover classes**

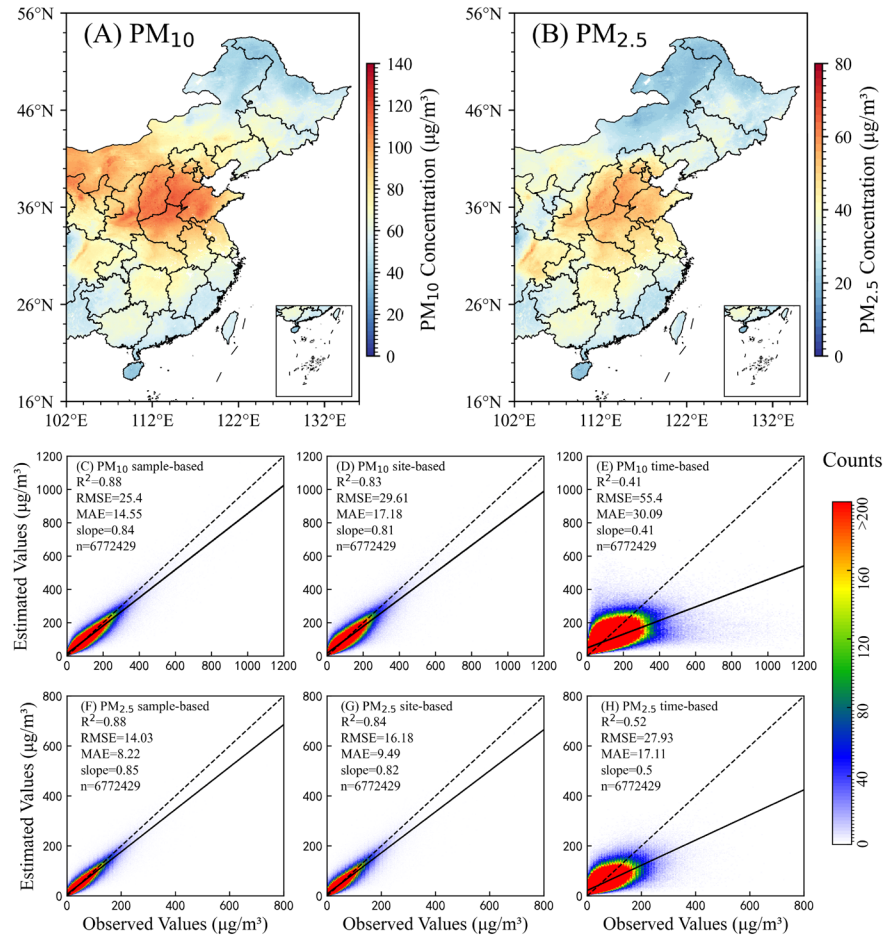
Urban-Rural Land Cover Class	Definition
Urban	50%<Urban grid
Suburban	25%<Urban grid<50%
Towns	12.5%<Urban grid<25%
High Agricultural Pressure Areas	50%<Cropland grid
Low Agricultural Pressure Areas	12.5%< Cropland grid grid<50%
Forests	50%<Forest grid
Grasslands	50%<Grassland grid
Other	Remaining unclassified grids (e.g., desert or tundra)

235 **3 Results**

236 **3.1 PM estimation model performance and PM distribution characteristics**

237 For the period from September 2015 to August 2023 in eastern China, a total of 6,772,429 samples
238 were matched. After parameter optimization and feature training, the optimal DOET model was derived,
239 and long-term time-series spatial distribution products for PM_{10} and $PM_{2.5}$ in eastern China were
240 generated. Figure 2 shows the results of 10-fold cross-validation based on sample, spatial and temporal
241 validations. Overall, the DOET model showed a high level of accuracy in the estimation of PM data. The
242 sample-based 10-fold cross-validation results (Figure 2C and 2F) yielded an R^2 of 0.87, with RMSE
243 (MAE) values of 25.82 (14.87) $\mu\text{g}/\text{m}^3$ for PM_{10} and 14.36 (8.44) $\mu\text{g}/\text{m}^3$ for $PM_{2.5}$. The slope of the fitting
244 line between observed and estimated values was 0.84. The performance of the DOET model in this study
245 is comparable to that reported in other studies that estimated PM using Himawari-8 TOAR data (Wang
246 et al., 2021; Chen et al., 2024b; Yin et al., 2021).

247 The 10-fold cross-validation results based on spatial and temporal validation were slightly lower
248 than those based on samples (Figures 2D-E and 2G-H). Spatial validation assessed the performance of
249 the model in estimating PM concentrations in areas without monitoring stations, after training the model
250 with samples from areas with stations. Temporal validation involved training the model with samples
251 from specific years and testing it with data from years not used in training. For these two validation
252 methods, the R^2 values for PM_{10} were 0.83 and 0.41, with RMSE values of 29.99 $\mu\text{g}/\text{m}^3$ and 55.44 $\mu\text{g}/\text{m}^3$,
253 respectively. For $PM_{2.5}$, the R^2 values were 0.83 and 0.52, with RMSE values of 16.46 $\mu\text{g}/\text{m}^3$ and 28.11
254 $\mu\text{g}/\text{m}^3$, respectively. **The DOET model is relatively robust based on sample and spatial validation results.**



255

256 **Figure 2. Spatial distribution of PM₁₀ and PM_{2.5} and cross validation results of the DOET model. The dashed**
257 **lines represent the 1:1 line, while the solid lines show the fitted line between observed and estimated values.**

258 By inputting TOAR, meteorological elements and geographical information into the optimally
259 parameterized DOET model, a pollutant estimation dataset for eastern China was generated for the period
260 September 2015 to August 2023. Due to the incomplete spatial coverage of TOAR data in different
261 months and hours (Song et al., 2024), the study first calculated monthly averages, which were then used
262 to derive annual averages. This step helps to minimize errors due to insufficient spatial coverage of the
263 samples (Ding et al., 2024). As shown in Figures 2A and 2B, the Beijing-Tianjin-Hebei region, the
264 Sichuan Basin, the Guanzhong region, and central China are hotspots for PM₁₀ and PM_{2.5} pollution (Wei
265 et al., 2021a), with concentrations reaching up to 100 µg/m³ for PM₁₀ and 60 µg/m³ for PM_{2.5}. In addition,
266 the Inner Mongolia region and northern Gansu, which are frequently affected by dust storms, are also
267 characterized by high PM₁₀ concentrations (Li et al., 2012). Overall, the PM₁₀ and PM_{2.5} concentrations
268 generated by the DOET model accurately reflect the spatial distribution characteristics of PM in eastern
269 China, and the estimation results are consistent with those of previous studies (Yang et al., 2023; Chen

270 et al., 2022b; Song et al., 2022a).

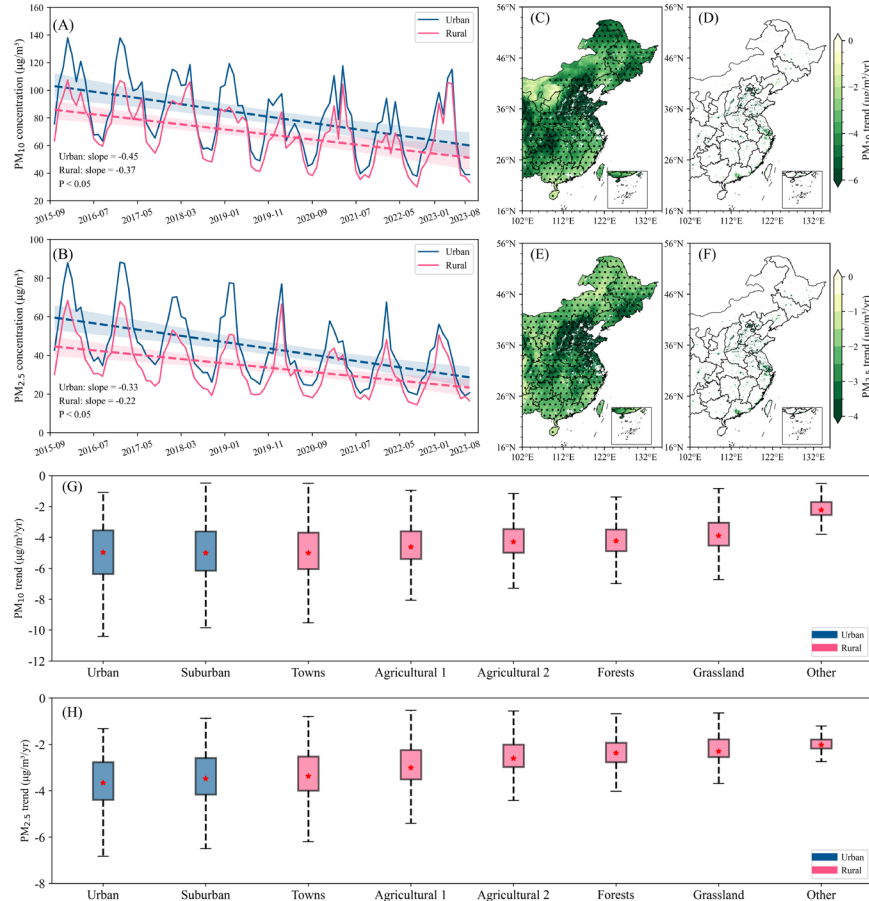
271 **3.2 Urban-rural differences in PM pollution trends in recent years**

272 The spatial distribution characteristics of PM_{10} and $PM_{2.5}$ trends from 2015 to 2023 were analysed,
273 and the results (Figures 3C-F) show a remarkable improvement of PM pollution in eastern China, as
274 indicated by a significant decreasing trend in PM concentrations. The average decrease for PM_{10} was -
275 $4.02 \pm 1.29 \mu\text{g}/\text{m}^3/\text{yr}$, while for $PM_{2.5}$, it was $-2.41 \pm 0.91 \mu\text{g}/\text{m}^3/\text{yr}$. However, this widespread decrease in
276 PM concentrations showed considerable spatial heterogeneity between urban and rural areas. The urban
277 and rural decrease trends for PM_{10} were $-4.99 \pm 1.68 \mu\text{g}/\text{m}^3/\text{yr}$ and $-3.98 \pm 1.26 \mu\text{g}/\text{m}^3/\text{yr}$, respectively,
278 while for $PM_{2.5}$, they were $-3.43 \pm 1.10 \mu\text{g}/\text{m}^3/\text{yr}$ and $-2.38 \pm 0.88 \mu\text{g}/\text{m}^3/\text{yr}$, respectively. This suggests
279 that the decrease in PM concentrations in rural areas was close to the regional average in eastern China,
280 while the decrease in urban areas was more pronounced than the overall trend. **We supplemented our**
281 **analysis by examining the relative change trends through benchmark concentration standardization.**
282 **Initially, the standard deviation of PM concentrations was computed for each grid point to assess spatial**
283 **variability. Subsequently, the annual mean PM data were used to calculate yearly relative changes**
284 **normalized against benchmark concentrations. Finally, a comprehensive trend analysis was performed**
285 **on these standardized values. The results are presented in Figure S2. Consistent with the overall trends**
286 **in PM concentrations, the relative change rates of $PM_{2.5}$ were quantified as $-38.24 \pm 3.40\%/\text{yr}$ in rural**
287 **areas and $-40.93 \pm 1.91\%/\text{yr}$ in urban areas. Similarly, PM_{10} exhibited relative change trends of -34.03**
288 **$\pm 6.55\%/\text{yr}$ (rural) and $-39.07 \pm 2.78\%/\text{yr}$ (urban). These findings demonstrate that, when accounting for**
289 **region-specific baseline concentrations across different land cover types, urban areas continue to show a**
290 **more substantial reduction in PM pollution compared to rural areas.**

291 From a broader perspective of the changes in particulate matter concentrations in eastern China, the
292 urban decrease trends for PM_{10} and $PM_{2.5}$ were $-0.47 \mu\text{g}/\text{m}^3/\text{month}$ and $-0.33 \mu\text{g}/\text{m}^3/\text{month}$, respectively,
293 while the rural decrease trends were $-0.37 \mu\text{g}/\text{m}^3/\text{month}$ and $-0.22 \mu\text{g}/\text{m}^3/\text{month}$, respectively. These
294 results indicate that the reduction trend in rural areas was slower than in urban areas. By 2023, particulate
295 matter concentrations in urban areas had decreased from about $20 \mu\text{g}/\text{m}^3$ higher than in rural areas to
296 levels almost equal to those in rural areas.

297 Urban and rural areas, categorized by land cover type, comprised eight different categories. The
298 study assessed their respective roles in PM concentration reduction trends and found that all eight

299 categories showed declining PM trends. However, the regions with the highest PM reduction trends were
 300 mainly four types: urban core areas, suburbs, towns and agricultural land 1 (high agricultural pressure).
 301 In contrast, the reduction trends were less pronounced in agricultural land 2 (low agricultural pressure),
 302 forests, grassland and other areas.

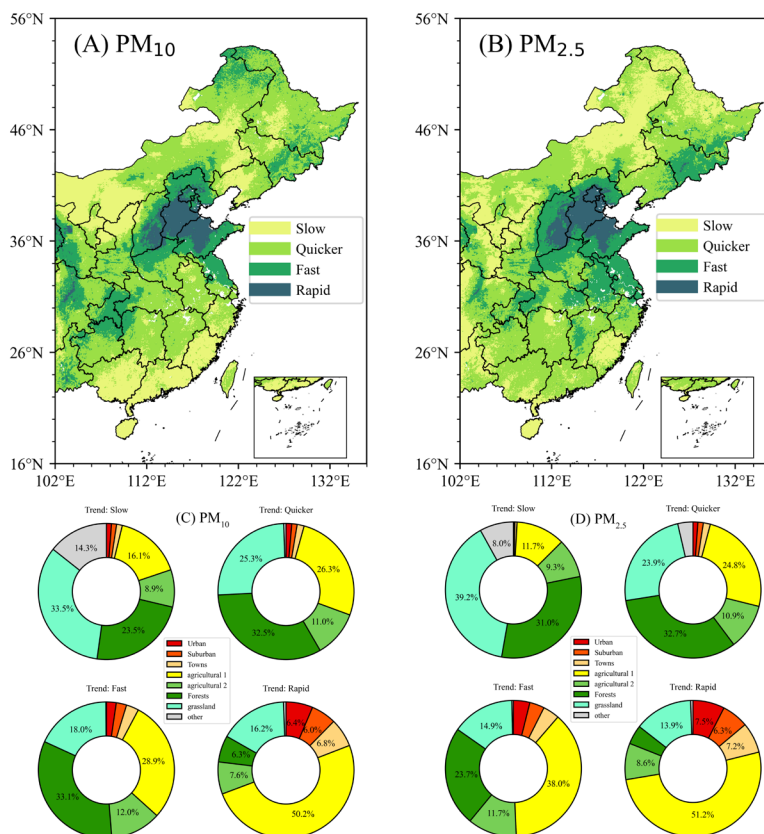


303 **Figure 3. Analysis of PM concentration trends in eastern China from September 2015 to August 2023.** Panels
 304 A, C, D, and G represent PM₁₀, while panels B, E, F, and H represent PM_{2.5}. In the legends of panels G-H,
 305 blue indicates urban areas, and red indicates rural areas. In G and H, the upper part of the box represents
 306 the upper quartile of the trend, and the lower part represents the lower quartile of the trend; the dotted line
 307 range represents the upper and lower limits of the trend values; the red dot represents the average value of
 308 the trend.

310 The trends in PM₁₀ and PM_{2.5} concentrations were categorized into four levels based on percentiles:
 311 slow decline (grid points with a decline trend below the 25th percentile), moderate decline (grid points
 312 with a decline trend between the 25th and 75th percentiles), rapid decline (grid points with a decline
 313 trend between the 75th and 95th percentiles), and sharp decline (grid points with a decline trend above
 314 the 95th percentile). As shown in Figure 4, the regions with the most significant changes in urban and
 315 rural PM trends are mainly concentrated in the Beijing-Tianjin-Hebei region, the Guanzhong region and

316 Central China.

317 In areas with slow and moderate declines, forests and grasslands accounted for the highest
318 proportions, ranging from 23.51% to 32.56% and 23.92% to 39.25%, respectively, followed by the
319 agricultural 1 and agricultural 2, which accounted for about 20%. In regions with rapid decline, the first
320 type of agricultural land had the highest proportion, ranging from 30 to 40%. Urban core, suburban and
321 towns had higher proportions in the fast decline regions, accounting for 6.44%, 6.01% and 6.83% of the
322 PM₁₀ decline trends and 7.52%, 6.34% and 7.21% of the PM_{2.5} decline trends respectively. In particular,
323 the agricultural 1 had the largest share in the strong decrease regions.



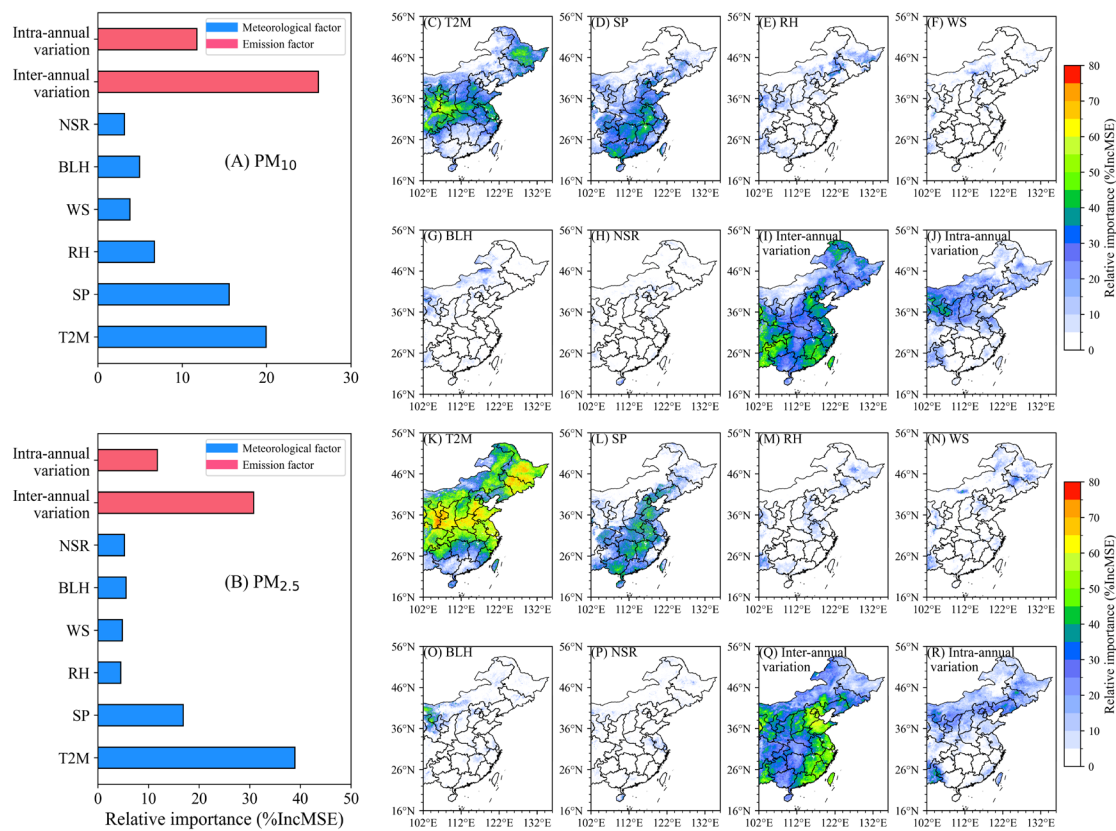
324
325 **Figure 4. Spatial distribution of particulate matter trend percentiles and pie charts. The individual color
326 scales in the figure represent different areas.**

327 **3.3 Assessing potential driving factors for PM pollution improvement and quantifying their
328 contributions**

329 A DOET model based on monthly PM data was developed to identify the key drivers of urban and
330 rural greening changes in China. Monthly mean PM₁₀ and PM_{2.5} concentrations were correlated with
331 meteorological factors and two temporal variables (year and month) representing the effects of
332 meteorological changes and anthropogenic influences, respectively (see Methods for details). The model

333 was cross-validated using a random training set (70%) and a validation set (30%). As shown in Figure
 334 S3, the DOET model explains more than 60% of the PM₁₀ trends and 80% of the PM_{2.5} trends in eastern
 335 China.

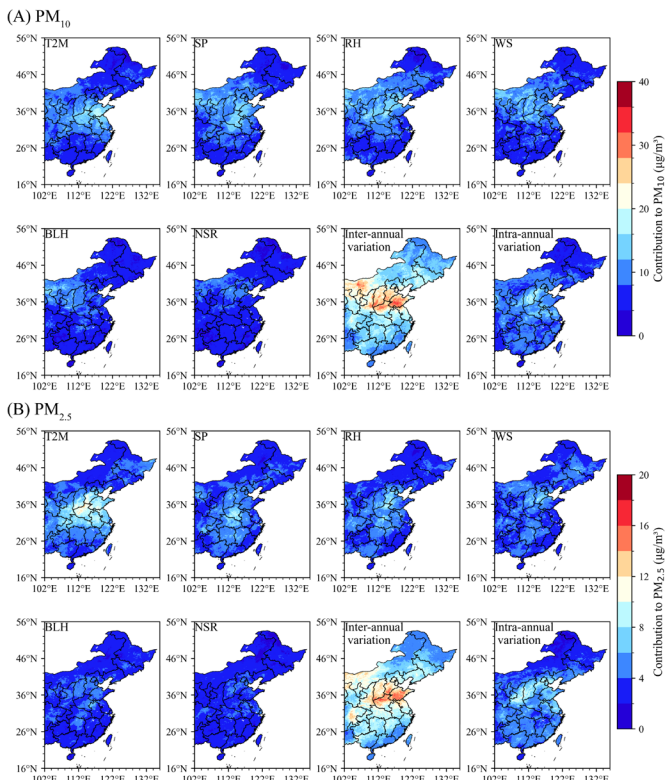
336 The relative importance of each variable in the DOET model was determined using the
 337 permutation_importance library. Inter-annual variability, intra-annual variability, air pressure and
 338 temperature were identified as significant contributors to the improvement of urban and rural PM
 339 pollution in eastern China (relative importance > 10%). Among them, interannual variability was the
 340 most influential factor for PM₁₀ (26.14±13.35%), followed by temperature (19.95±15.06%) (Figure 5A).
 341 In contrast, for PM_{2.5}, interannual variability ranked second (30.79±12.86%), while temperature had a
 342 stronger effect (38.90±17.73%) (Figure 5B). The spatial distribution of the relative importance of the
 343 four main contributing factors, shown in Figures 5C-R, indicates that regions with high relative
 344 importance values overlapped with PM pollution hotspots. Furthermore, as shown in Figure S4, the
 345 driving factors for urban and rural PM pollution improvement differed significantly between land cover
 346 types.



348 **Figure 5. Spatial distribution of the relative influence of each variable on PM pollution. In panels (A-B), the**
 349 **red variables are related to emissions and the blue variables are related to meteorology.**

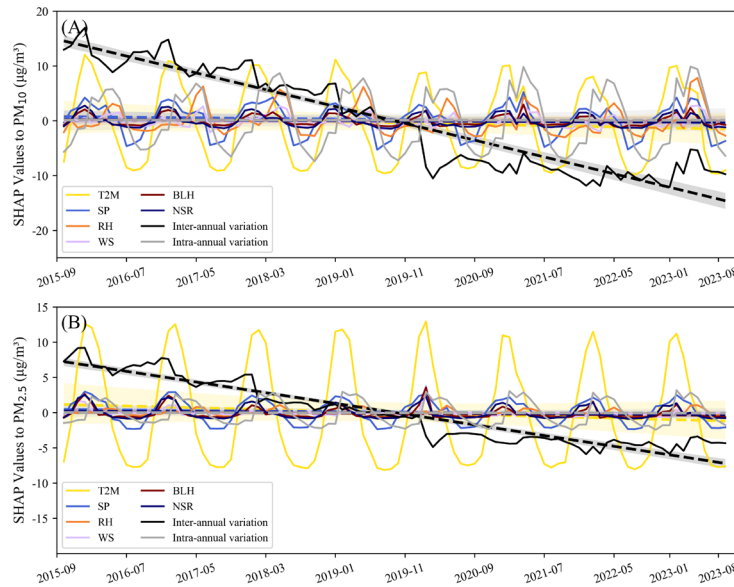
350 The relative contributions of each variable in the DOET model to the PM concentration values were
351 obtained using the permutation_importance library. The results showed that the improvement in urban
352 and rural PM pollution was primarily driven by interannual variation (Figure 5), followed by temperature,
353 which is consistent with the relative importance results in Figure 5. Figure S5-S6 illustrate how variations
354 in the values of the driving factors influence their relative contributions to PM concentrations. In
355 particular, PM concentrations showed a clear inverse relationship with temperature and interannual
356 variations, especially for PM_{2.5}. Relative humidity also showed clear differences in its contribution to
357 PM₁₀ and PM_{2.5}: lower relative humidity was associated with higher PM₁₀ concentrations, whereas higher
358 PM_{2.5} concentrations were associated with higher relative humidity. The scatter plots illustrating the
359 relationships between other variables and their relative contributions to PM are shown in Figures S4-S5.

360 Figure 6 shows the relative contributions of each variable, with the spatial distribution patterns of
361 interannual variations being particularly noteworthy. For PM₁₀, regions such as Guanzhong, North China,
362 and Inner Mongolia were more susceptible to the influence of interannual variations. We hypothesize
363 that the improvement in PM₁₀ pollution be due not only be attributed to anthropogenic emission
364 reductions but also to sandstorm events in recent years, which are important sources of PM₁₀ (Wang et
365 al., 2024c). However, the explanatory power of the model for PM₁₀ trends in these areas remains
366 relatively low, suggesting the need for further investigation into the specific causes. For PM_{2.5}, the impact
367 of interannual variability was observed mainly in the Guanzhong region, North China, and the Sichuan
368 Basin, all of which are key areas for pollution control (Wang et al., 2022a; Yu et al., 2022). Contrary to
369 the relative importance results, the dominant factor driving the improvement in urban and rural PM
370 pollution was the influence of interannual variability (Figure S7), with other variables showing varying
371 effects across different land cover types.



372
373 **Figure 6. The spatial distribution of the relative contributions of each variable to PM pollution**

374 Finally, the “tree_SHAP” tool was used to decompose the SHAP values of each variable in the
 375 DOET model. By analyzing the positive and negative changes in the SHAP values, the influence of each
 376 variable on the PM pollution improvement - whether positive or negative - was quantified, thus
 377 complementing the assessment of driving factor contributions (Li et al., 2024a). As shown in Figure 7,
 378 the SHAP values show a strong negative correlation between PM concentrations and the contribution of
 379 interannual variability in eastern China. In particular, during the transition from 2019 to 2020, the
 380 contribution of interannual variations to PM concentrations shifted critically from positive to negative.
 381 Interestingly, despite the high relative importance and contribution of some variables, their SHAP values
 382 showed periodic fluctuations, alternating between positive and negative, such as for temperature (with a
 383 negative contribution in summer and a positive one in winter). This suggests that meteorological factors
 384 influence PM concentrations in a periodic manner, while the only factor that consistently contributes to
 385 the improvement of PM pollution is the interannual variation driven by anthropogenic influences. The
 386 Figure S8-S9 show the SHAP values of various variables for PM in urban and rural areas, respectively.
 387 The impact of various variables, including temperature, on PM is primarily evident in urban areas, where
 388 the magnitude of the values and the rate of change are both higher than in rural areas.



389

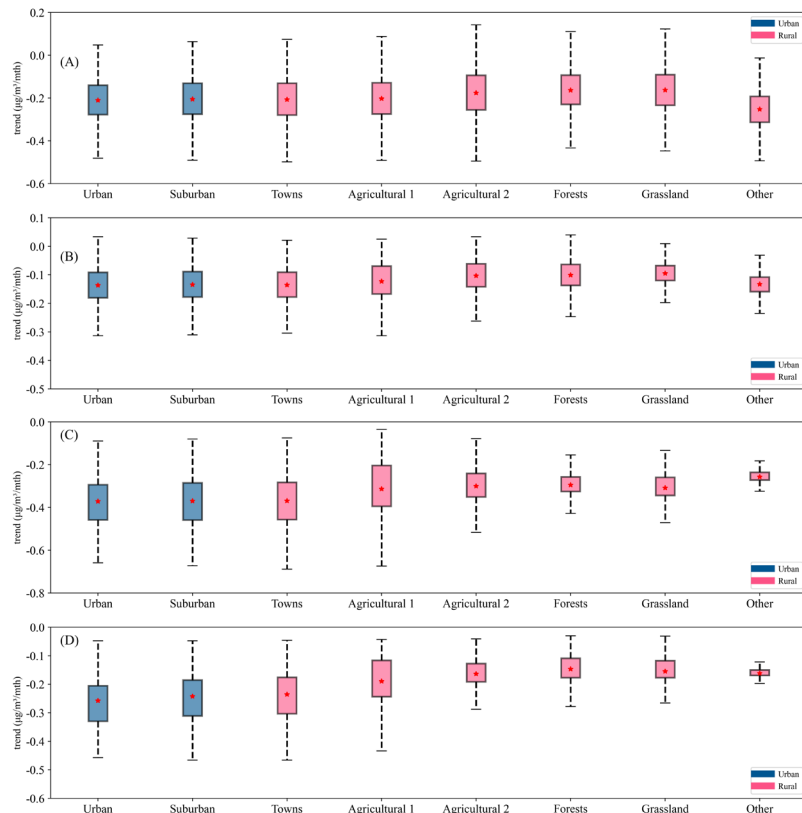
390 **Figure 7. The SHAP values of each variable for PM. The solid line represents the SHAP values, and the dashed
391 line indicates their trend of change.**

392 **3.5 Trends in the contribution of driving factors to PM pollution improvement**

393 To further investigate the influence of potential driving factors on PM concentrations, we conducted
394 a detailed analysis of the trends in the contributions of each variable was performed. As shown in Figures
395 S10-S13, the monthly trends in the relative contributions and SHAP values of each variable were
396 examined, categorized into significant changes ($p < 0.05$) and non-significant changes ($p > 0.05$). For the
397 relative contributions (including PM_{10} and $PM_{2.5}$), with the exception of interannual variations, all other
398 variables showed a decreasing trend, although some regions showed an increasing trend. However, the
399 contribution of interannual variability showed a significant decrease, indicating a reduced capacity of
400 anthropogenic emissions to trigger PM pollution events. This phenomenon is more pronounced for the
401 trends in SHAP values. In particular, only the contribution of interannual variations showed a significant
402 decreasing trend, while the other variables showed non-significant decreasing trends, mainly due to the
403 periodic variations in their contributions, as shown in Figure 7. This shows that the impact of a variable
404 on PM pollution cannot only be assessed on the basis of its relative contribution, but its positive or
405 negative influence on the improvement of PM pollution must also be considered.

406 Given the significant decrease in the contribution of interannual variation, we further compared its
407 trends across different land cover types in urban and rural areas, as this variable plays the most important
408 role in PM pollution improvement. As shown in Figure 8 (A-B), the trends in relative contributions for

409 both PM_{10} and $PM_{2.5}$ did not differ significantly between the eight land cover types, although urban areas
 410 showed the highest rate of decrease. However, the trends in SHAP values shown in Figures 8 (C-D)
 411 revealed that the reduction in the contribution of interannual variation was most pronounced in urban
 412 core areas, suburban areas, and towns. In contrast, the decrease in interannual contributions was more
 413 pronounced in agricultural areas than in urban areas, while other rural areas showed a weaker influence
 414 of interannual variations on PM pollution improvement. These results suggest that the improvement in
 415 PM pollution in urban areas is more closely related to anthropogenic influences, whereas this relationship
 416 is less pronounced in rural areas.



417
 418 **Figure 8. Trends in the relative contribution (A-B) and SHAP values (C-D) of interannual variability of**
 419 **different land cover types. A and C represent the case for PM_{10} , while B and D represent the case for $PM_{2.5}$.**
 420 **In the legend, blue represents urban areas, and red represents rural areas. In Figure 8, the upper part of the**
 421 **box represents the upper quartile of the trend, and the lower part represents the lower quartile of the trend;**
 422 **the dotted line range represents the upper and lower limits of the trend values; the red dot represents the**
 423 **average value of the trend.**

424

425 **4 Discussion and conclusion**

426 Due to the predominant distribution of environmental quality monitoring stations in urban areas

427 (Park et al., 2020), discussions on air pollution patterns between urban and rural regions have been
428 limited (Hammer et al., 2020). In this study, we used a regression-based machine learning DOET
429 algorithm to integrate station-observed PM concentrations, satellite-observed TOAR, meteorological
430 factors, and geographic information data. This approach enabled us to generate long-term, high spatio-
431 temporal resolution datasets of near-surface PM₁₀ and PM_{2.5}, with a spatial resolution of 5 km, an hourly
432 temporal resolution, and coverage across the entire eastern China region. Using the generated PM data
433 in conjunction with a constructed urban-rural land type framework, we successfully captured the broad
434 trends and patterns of PM₁₀ and PM_{2.5} concentration changes from urban and suburban areas to different
435 types of rural regions.

436 Based on the estimated dataset and interpretable parameters, the study identified significant large-
437 scale improvements in PM pollution in eastern China from 2015 to 2023, indicating notable
438 achievements from the implementation of clean air measures. The study noted that the second phase of
439 the clean air action plan, implemented from 2018 to 2020, also produced positive results, following the
440 success of the first phase from 2013 to 2017 (Geng et al., 2024). Our results show that under the urban-
441 rural framework, PM reductions are generally higher in urban areas than in rural areas. However, the
442 highly polluted agricultural areas in rural regions also showed significant improvements in PM pollution.
443 In fact, during air pollution prevention and control efforts, China's main emission reduction measures
444 focused on coal consumption and energy-intensive industries such as steel and cement, and these
445 measures were often effective in urban areas (Yun et al., 2020; Huang et al., 2014b; Wang et al., 2013).
446 This does not mean that rural areas have been neglected, as evidenced by reductions in biomass burning
447 (Shen et al., 2019). The finding that interannual variability is the main driver of PM pollution
448 improvement is consistent with these facts. It is worth noting that the rate of PM concentration decline
449 is faster in urban areas than in rural areas, bringing the concentration levels of the two areas closer
450 together. Given the more pronounced decrease in the contribution of inter-annual variations in urban
451 areas, future efforts to prevent and control air pollution should maintain the current intensity or balance
452 investments between urban and rural areas.

453 Our results indicate that meteorological factors with distinct seasonal variations, such as
454 temperature, boundary layer height, and relative humidity, have a cyclical influence on PM pollution.
455 For example, summer weather conditions, such as abundant precipitation, high relative humidity and

456 abundant water vapour favour PM dispersion, while winter weather conditions are less conducive to
457 pollutant dispersion and spring is often characterised by frequent dust events. Therefore, due to their
458 periodic positive and negative contributions and variability, meteorological conditions do not provide
459 stable improvements in PM pollution. Moreover, the contribution of meteorological conditions to PM
460 concentrations does not show a significant trend. Thus, given the high contribution of inter-annual
461 variability to the improvement of PM pollution, the impact of meteorological conditions on the inter-
462 annual variability of PM pollution in China should not be overemphasised.

463 Although this study evaluated the patterns of PM pollution improvement and its driving factors in
464 urban and rural areas of eastern China, the contribution of interannual variations driven by anthropogenic
465 influences was represented by a time variable in our analysis. In the future, key factors driving changes
466 in air pollutants, such as energy management, urban traffic management, agricultural nitrogen deposition
467 effects and biomass burning, need to be further incorporated into the attribution analysis to distinguish
468 and quantify the contributions of different anthropogenic emission reduction measures to PM pollution
469 improvement. Given the different drivers of PM pollution improvement in urban and rural areas, it is
470 essential to implement tailored strategies in both regions to achieve more effective and comprehensive
471 air pollution prevention and control measures in the future.

472 **Data availability**

473 The hourly ground station observations of near-surface PM₁₀ and PM_{2.5} concentrations are obtained from
474 the China National Environmental Monitoring Center (CNEMC), which can be accessed on its official
475 website (<http://www.cnemc.cn/en/>). Himawari-8 TOAR data provided by the Japan Meteorological
476 Agency, download from: <http://www.eorc.jaxa.jp/ptrec/index.html>. Meteorological variables were
477 derived from the reanalysis data set provided by the European Centre for Medium-Range Weather
478 Forecasts (ECMWF) (<https://cds.climate.copernicus.eu/cdsapp#!/search?type=dataset>). MODIS Land
479 use/cover change (LUCC) product can be downloaded from
480 <https://doi.org/10.5067/MODIS/MCD12C1.061>. The 2015 UN-adjusted population density data (RK)
481 can be downloaded from <https://doi.org/10.7927/H4PN93PB>. SRTM-3 elevation data jointly measured
482 by NASA and the U.S. Department of Defense's National Imagery and Mapping Agency (NIMA)
483 (HEIGHT) can be downloaded from <https://doi.org/10.5067/MEaSUREs/SRTM/SRTMGL3.003>. The

484 particulate matter data generated in the manuscript can be obtained at the following URL:
485 <https://doi.org/10.5281/zenodo.17090707>.

486 **Code availability**

487 The codes are available from the corresponding author upon request.

488 **Acknowledgements**

489 We would like to express our gratitude to the China National Environmental Monitoring Center,
490 Japan Meteorological Agency, European Centre for Medium-Range Weather Forecasts, and NASA
491 for their datasets.

492 **Financial support**

493 The work was supported by the Noncommunicable Chronic Diseases-National Science and Technology
494 Major Project (Grant number 2024ZD0531600), the National Natural Science Foundation of China
495 (Grant number 42427803), the Gansu Provincial Science and Technology Plan (Grant number
496 25RCKA024), and the Fundamental Research Funds for the Central Universities (Grant number lzujbky-
497 2023-ey10).

498 **Author contributions**

499 Z.S.: Software, Methodology, Data curation, Writing-Original draft preparation, Formal Analysis,
500 Visualization. B.C.: Conceptualization, Methodology, Writing-Reviewing and Editing, Resources.

501 **Competing interests**

502 The authors declare that they have no conflict of interest.

503 **References**

504 An, Z., Huang, R.-J., Zhang, R., Tie, X., Li, G., Cao, J., Zhou, W., Shi, Z., Han, Y., Gu, Z., and Ji, Y.:
505 Severe haze in northern China: A synergy of anthropogenic emissions and atmospheric processes,
506 Proceedings of the National Academy of Sciences, 116, 8657-8666,
507 <https://doi.org/10.1073/pnas.1900125116>, 2019.
508 Apte, J. S., Marshall, J. D., Cohen, A. J., and Brauer, M.: Addressing Global Mortality from Ambient

509 PM2.5, Environmental Science & Technology, 49, 8057-8066, <https://doi.org/10.1021/acs.est.5b01236>,
510 2015.

511 Berner, L. T., Massey, R., Jantz, P., Forbes, B. C., Macias-Fauria, M., Myers-Smith, I., Kumpula, T.,
512 Gauthier, G., Andreu-Hayles, L., Gaglioti, B. V., Burns, P., Zetterberg, P., D'Arrigo, R., and Goetz, S. J.:
513 Summer warming explains widespread but not uniform greening in the Arctic tundra biome, Nature
514 Communications, 11, 4621, <https://doi.org/10.1038/s41467-020-18479-5>, 2020.

515 Bessho, K., Date, K., Hayashi, M., Ikeda, A., Imai, T., Inoue, H., Kumagai, Y., Miyakawa, T., Murata,
516 H., Ohno, T., Okuyama, A., Oyama, R., Sasaki, Y., Shimazu, Y., Shimoji, K., Sumida, Y., Suzuki, M.,
517 Taniguchi, H., Tsuchiyama, H., Uesawa, D., Yokota, H., and Yoshida, R.: An Introduction to Himawari-
518 8/9—Japan's New-Generation Geostationary Meteorological Satellites, Journal of the
519 Meteorological Society of Japan. Ser. II, 94, 151-183, <https://doi.org/10.2151/jmsj.2016-009>, 2016.

520 Brauer, M., Freedman, G., Frostad, J., van Donkelaar, A., Martin, R. V., Dentener, F., Dingenen, R. v.,
521 Estep, K., Amini, H., Apte, J. S., Balakrishnan, K., Barregard, L., Broday, D., Feigin, V., Ghosh, S.,
522 Hopke, P. K., Knibbs, L. D., Kokubo, Y., Liu, Y., Ma, S., Morawska, L., Sangrador, J. L. T., Shaddick,
523 G., Anderson, H. R., Vos, T., Forouzanfar, M. H., Burnett, R. T., and Cohen, A.: Ambient Air Pollution
524 Exposure Estimation for the Global Burden of Disease 2013, Environmental Science & Technology, 50,
525 79-88, <https://doi.org/10.1021/acs.est.5b03709>, 2016.

526 Burnett, R., Chen, H., Szyszkowicz, M., Fann, N., Hubbell, B., Pope, C. A., Apte, J. S., Brauer, M.,
527 Cohen, A., Weichenthal, S., Coggins, J., Di, Q., Brunekreef, B., Frostad, J., Lim, S. S., Kan, H., Walker,
528 K. D., Thurston, G. D., Hayes, R. B., Lim, C. C., Turner, M. C., Jerrett, M., Krewski, D., Gapstur, S. M.,
529 Diver, W. R., Ostro, B., Goldberg, D., Crouse, D. L., Martin, R. V., Peters, P., Pinault, L., Tjepkema, M.,
530 van Donkelaar, A., Villeneuve, P. J., Miller, A. B., Yin, P., Zhou, M., Wang, L., Janssen, N. A. H., Marra,
531 M., Atkinson, R. W., Tsang, H., Quoc Thach, T., Cannon, J. B., Allen, R. T., Hart, J. E., Laden, F.,
532 Cesaroni, G., Forastiere, F., Weinmayr, G., Jaensch, A., Nagel, G., Concin, H., and Spadaro, J. V.: Global
533 estimates of mortality associated with long-term exposure to outdoor fine particulate matter, Proceedings
534 of the National Academy of Sciences, 115, 9592-9597, <https://doi.org/10.1073/pnas.1803222115>, 2018.

535 Burnett Richard, T., Pope, C. A., Ezzati, M., Olives, C., Lim Stephen, S., Mehta, S., Shin Hwashin, H.,
536 Singh, G., Hubbell, B., Brauer, M., Anderson, H. R., Smith Kirk, R., Balmes John, R., Bruce Nigel, G.,
537 Kan, H., Laden, F., Prüss-Ustün, A., Turner Michelle, C., Gapstur Susan, M., Diver, W. R., and Cohen,
538 A.: An Integrated Risk Function for Estimating the Global Burden of Disease Attributable to Ambient
539 Fine Particulate Matter Exposure, Environmental Health Perspectives, 122, 397-403,
540 <https://doi.org/10.1289/ehp.1307049>, 2014.

541 Cao, B. and Yin, Z.: Future atmospheric circulations benefit ozone pollution control in Beijing-Tianjin-
542 Hebei with global warming, Science of The Total Environment, 743, 140645,
543 <https://doi.org/10.1016/j.scitotenv.2020.140645>, 2020.

544 Chen, B., Hu, J., and Wang, Y.: Synergistic observation of FY-4A&4B to estimate CO concentration in
545 China: combining interpretable machine learning to reveal the influencing mechanisms of CO variations,
546 npj Climate and Atmospheric Science, 7, 9, <https://doi.org/10.1038/s41612-023-00559-0>, 2024a.

547 Chen, B., Song, Z., Pan, F., and Huang, Y.: Obtaining vertical distribution of PM2.5 from CALIOP data
548 and machine learning algorithms, Science of The Total Environment, 805, 150338,
549 <https://doi.org/10.1016/j.scitotenv.2021.150338>, 2022a.

550 Chen, B., Song, Z., Shi, B., and Li, M.: An interpretable deep forest model for estimating hourly PM10
551 concentration in China using Himawari-8 data, Atmospheric Environment, 268, 118827,
552 <https://doi.org/10.1016/j.atmosenv.2021.118827>, 2022b.

553 Chen, B., Wang, Y., Huang, J., Zhao, L., Chen, R., Song, Z., and Hu, J.: Estimation of near-surface ozone
554 concentration and analysis of main weather situation in China based on machine learning model and
555 Himawari-8 TOAR data, *Science of The Total Environment*, 864, 160928,
556 <https://doi.org/10.1016/j.scitotenv.2022.160928>, 2023.

557 Chen, B., Song, Z., Huang, J., Zhang, P., Hu, X., Zhang, X., Guan, X., Ge, J., and Zhou, X.: Estimation
558 of Atmospheric PM10 Concentration in China Using an Interpretable Deep Learning Model and Top-of-
559 the-Atmosphere Reflectance Data From China's New Generation Geostationary Meteorological Satellite,
560 FY-4A, *Journal of Geophysical Research: Atmospheres*, 127, e2021JD036393,
561 <https://doi.org/10.1029/2021JD036393>, 2022c.

562 Chen, C.-C., Wang, Y.-R., Yeh, H.-Y., Lin, T.-H., Huang, C.-S., and Wu, C.-F.: Estimating monthly PM2.5
563 concentrations from satellite remote sensing data, meteorological variables, and land use data using
564 ensemble statistical modeling and a random forest approach, *Environmental Pollution*, 291, 118159,
565 <https://doi.org/10.1016/j.envpol.2021.118159>, 2021.

566 Chen, G., Li, S., Knibbs, L. D., Hamm, N. A. S., Cao, W., Li, T., Guo, J., Ren, H., Abramson, M. J., and
567 Guo, Y.: A machine learning method to estimate PM2.5 concentrations across China with remote sensing,
568 meteorological and land use information, *Science of The Total Environment*, 636, 52-60,
569 <https://doi.org/10.1016/j.scitotenv.2018.04.251>, 2018a.

570 Chen, J., Yin, J., Zang, L., Zhang, T., and Zhao, M.: Stacking machine learning model for estimating
571 hourly PM2.5 in China based on Himawari 8 aerosol optical depth data, *Science of The Total
572 Environment*, 697, 134021, <https://doi.org/10.1016/j.scitotenv.2019.134021>, 2019a.

573 Chen, J., Li, Z., Lv, M., Wang, Y., Wang, W., Zhang, Y., Wang, H., Yan, X., Sun, Y., and Cribb, M.:
574 Aerosol hygroscopic growth, contributing factors, and impact on haze events in a severely polluted
575 region in northern China, *Atmos. Chem. Phys.*, 19, 1327-1342, <https://doi.org/10.5194/acp-19-1327-2019>, 2019b.

576 Chen, L., Zhu, J., Liao, H., Yang, Y., and Yue, X.: Meteorological influences on PM2.5 and O3 trends
577 and associated health burden since China's clean air actions, *Science of The Total Environment*, 744,
578 140837, <https://doi.org/10.1016/j.scitotenv.2020.140837>, 2020a.

579 Chen, S., Guo, J., Song, L., Li, J., Liu, L., and Cohen, J. B.: Inter-annual variation of the spring haze
580 pollution over the North China Plain: Roles of atmospheric circulation and sea surface temperature,
581 *International Journal of Climatology*, 39, 783-798, <https://doi.org/10.1002/joc.5842>, 2019c.

582 Chen, X., Zhang, W., He, J., Zhang, L., Guo, H., Li, J., and Gu, X.: Mapping PM2.5 concentration from
583 the top-of-atmosphere reflectance of Himawari-8 via an ensemble stacking model, *Atmospheric
584 Environment*, 330, 120560, <https://doi.org/10.1016/j.atmosenv.2024.120560>, 2024b.

585 Chen, Z., Xie, X., Cai, J., Chen, D., Gao, B., He, B., Cheng, N., and Xu, B.: Understanding
586 meteorological influences on PM2.5 concentrations across China: a temporal and spatial perspective,
587 *Atmos. Chem. Phys.*, 18, 5343-5358, <https://doi.org/10.5194/acp-18-5343-2018>, 2018b.

588 Chen, Z., Chen, D., Zhao, C., Kwan, M.-p., Cai, J., Zhuang, Y., Zhao, B., Wang, X., Chen, B., Yang, J.,
589 Li, R., He, B., Gao, B., Wang, K., and Xu, B.: Influence of meteorological conditions on PM2.5
590 concentrations across China: A review of methodology and mechanism, *Environment International*, 139,
591 105558, <https://doi.org/10.1016/j.envint.2020.105558>, 2020b.

592 Cheng, J., Tong, D., Zhang, Q., Liu, Y., Lei, Y., Yan, G., Yan, L., Yu, S., Cui, R. Y., Clarke, L., Geng, G.,
593 Zheng, B., Zhang, X., Davis, S. J., and He, K.: Pathways of China's PM2.5 air quality 2015–2060 in the
594 context of carbon neutrality, *National Science Review*, 8, nwab078, <https://doi.org/10.1093/nsr/nwab078>,
595 2021.

596

597 Cohen, A. J., Brauer, M., Burnett, R., Anderson, H. R., Frostad, J., Estep, K., Balakrishnan, K.,
598 Brunekreef, B., Dandona, L., Dandona, R., Feigin, V., Freedman, G., Hubbell, B., Jobling, A., Kan, H.,
599 Knibbs, L., Liu, Y., Martin, R., Morawska, L., Pope, C. A., Shin, H., Straif, K., Shaddick, G., Thomas,
600 M., van Dingenen, R., van Donkelaar, A., Vos, T., Murray, C. J. L., and Forouzanfar, M. H.: Estimates
601 and 25-year trends of the global burden of disease attributable to ambient air pollution: an analysis of
602 data from the Global Burden of Diseases Study 2015, *The Lancet*, 389, 1907-1918,
603 [https://doi.org/10.1016/S0140-6736\(17\)30505-6](https://doi.org/10.1016/S0140-6736(17)30505-6), 2017.

604 Dai, Q., Hou, L., Liu, B., Zhang, Y., Song, C., Shi, Z., Hopke, P. K., and Feng, Y.: Spring Festival and
605 COVID-19 Lockdown: Disentangling PM Sources in Major Chinese Cities, *Geophysical Research
606 Letters*, 48, e2021GL093403, <https://doi.org/10.1029/2021GL093403>, 2021.

607 Ding, Y., Li, S., Xing, J., Li, X., Ma, X., Song, G., Teng, M., Yang, J., Dong, J., and Meng, S.: Retrieving
608 hourly seamless PM_{2.5} concentration across China with physically informed spatiotemporal connection,
609 *Remote Sensing of Environment*, 301, 113901, <https://doi.org/10.1016/j.rse.2023.113901>, 2024.

610 Geng, G., Xiao, Q., Zheng, Y., Tong, D., Zhang, Y., Zhang, X., Zhang, Q., He, K., and Liu, Y.: Impact of
611 China's Air Pollution Prevention and Control Action Plan on PM_{2.5} chemical composition over eastern
612 China, *Science China Earth Sciences*, 62, 1872-1884, <https://doi.org/10.1007/s11430-018-9353-x>, 2019.

613 Geng, G., Liu, Y., Liu, Y., Liu, S., Cheng, J., Yan, L., Wu, N., Hu, H., Tong, D., Zheng, B., Yin, Z., He,
614 K., and Zhang, Q.: Efficacy of China's clean air actions to tackle PM_{2.5} pollution between 2013 and
615 2020, *Nature Geoscience*, 17, 987-994, 10.1038/s41561-024-01540-z, 2024.

616 Geng, G., Xiao, Q., Liu, S., Liu, X., Cheng, J., Zheng, Y., Xue, T., Tong, D., Zheng, B., Peng, Y., Huang,
617 X., He, K., and Zhang, Q.: Tracking Air Pollution in China: Near Real-Time PM_{2.5} Retrievals from
618 Multisource Data Fusion, *Environmental Science & Technology*, 55, 12106-12115,
619 10.1021/acs.est.1c01863, 2021.

620 Geurts, P., Ernst, D., and Wehenkel, L.: Extremely randomized trees, *Machine Learning*, 63, 3-42,
621 <https://doi.org/10.1007/s10994-006-6226-1>, 2006.

622 Grange, S. K. and Carslaw, D. C.: Using meteorological normalisation to detect interventions in air
623 quality time series, *Science of The Total Environment*, 653, 578-588,
624 <https://doi.org/10.1016/j.scitotenv.2018.10.344>, 2019.

625 Gui, K., Che, H., Wang, Y., Wang, H., Zhang, L., Zhao, H., Zheng, Y., Sun, T., and Zhang, X.: Satellite-
626 derived PM_{2.5} concentration trends over Eastern China from 1998 to 2016: Relationships to emissions
627 and meteorological parameters, *Environmental Pollution*, 247, 1125-1133,
628 <https://doi.org/10.1016/j.envpol.2019.01.056>, 2019.

629 Hammer, M. S., van Donkelaar, A., Li, C., Lyapustin, A., Sayer, A. M., Hsu, N. C., Levy, R. C., Garay,
630 M. J., Kalashnikova, O. V., Kahn, R. A., Brauer, M., Apte, J. S., Henze, D. K., Zhang, L., Zhang, Q.,
631 Ford, B., Pierce, J. R., and Martin, R. V.: Global Estimates and Long-Term Trends of Fine Particulate
632 Matter Concentrations (1998–2018), *Environmental Science & Technology*, 54, 7879-7890,
633 10.1021/acs.est.0c01764, 2020.

634 He, J., Gong, S., Yu, Y., Yu, L., Wu, L., Mao, H., Song, C., Zhao, S., Liu, H., Li, X., and Li, R.: Air
635 pollution characteristics and their relation to meteorological conditions during 2014–2015 in major
636 Chinese cities, *Environmental Pollution*, 223, 484-496, <https://doi.org/10.1016/j.envpol.2017.01.050>,
637 2017.

638 He, Q., Cao, J., Saide, P. E., Ye, T., and Wang, W.: Unraveling the Influence of Satellite-Observed Land
639 Surface Temperature on High-Resolution Mapping of Ground-Level Ozone Using Interpretable Machine
640 Learning, *Environmental Science & Technology*, 58, 15938-15948,

641 <https://doi.org/10.1021/acs.est.4c02926>, 2024.

642 Hersbach, H., Bell, B., Berrisford, P., Hirahara, S., Horányi, A., Muñoz-Sabater, J., Nicolas, J., Peubey, C., Radu, R., Schepers, D., Simmons, A., Soci, C., Abdalla, S., Abellan, X., Balsamo, G., Bechtold, P., Biavati, G., Bidlot, J., Bonavita, M., De Chiara, G., Dahlgren, P., Dee, D., Diamantakis, M., Dragani, R., Flemming, J., Forbes, R., Fuentes, M., Geer, A., Haimberger, L., Healy, S., Hogan, R. J., Hólm, E., Janisková, M., Keeley, S., Laloyaux, P., Lopez, P., Lupu, C., Radnoti, G., de Rosnay, P., Rozum, I., Vamborg, F., Villaume, S., and Thépaut, J.-N.: The ERA5 global reanalysis, *Quarterly Journal of the Royal Meteorological Society*, 146, 1999-2049, <https://doi.org/10.1002/qj.3803>, 2020.

643 Hou, L., Dai, Q., Song, C., Liu, B., Guo, F., Dai, T., Li, L., Liu, B., Bi, X., Zhang, Y., and Feng, Y.: Revealing Drivers of Haze Pollution by Explainable Machine Learning, *Environmental Science & Technology Letters*, 9, 112-119, <https://doi.org/10.1021/acs.estlett.1c00865>, 2022.

644 Hu, Y., Zeng, C., Li, T., and Shen, H.: Performance comparison of Fengyun-4A and Himawari-8 in PM2.5 estimation in China, *Atmospheric Environment*, 271, 118898, <https://doi.org/10.1016/j.atmosenv.2021.118898>, 2022.

645 Hua, J., Zhang, Y., de Foy, B., Mei, X., Shang, J., and Feng, C.: Competing PM2.5 and NO₂ holiday effects in the Beijing area vary locally due to differences in residential coal burning and traffic patterns, *Science of The Total Environment*, 750, 141575, <https://doi.org/10.1016/j.scitotenv.2020.141575>, 2021.

646 Huang, C., Hu, J., Xue, T., Xu, H., and Wang, M.: High-Resolution Spatiotemporal Modeling for Ambient PM2.5 Exposure Assessment in China from 2013 to 2019, *Environmental Science & Technology*, 55, 2152-2162, 10.1021/acs.est.0c05815, 2021.

647 Huang, R.-J., Zhang, Y., Bozzetti, C., Ho, K.-F., Cao, J.-J., Han, Y., Daellenbach, K. R., Slowik, J. G., Platt, S. M., Canonaco, F., Zotter, P., Wolf, R., Pieber, S. M., Bruns, E. A., Crippa, M., Ciarelli, G., Piazzalunga, A., Schwikowski, M., Abbaszade, G., Schnelle-Kreis, J., Zimmermann, R., An, Z., Szidat, S., Baltensperger, U., Haddad, I. E., and Prévôt, A. S. H.: High secondary aerosol contribution to particulate pollution during haze events in China, *Nature*, 514, 218-222, <https://doi.org/10.1038/nature13774>, 2014a.

648 Huang, Y., Shen, H., Chen, H., Wang, R., Zhang, Y., Su, S., Chen, Y., Lin, N., Zhuo, S., Zhong, Q., Wang, X., Liu, J., Li, B., Liu, W., and Tao, S.: Quantification of Global Primary Emissions of PM2.5, PM10, and TSP from Combustion and Industrial Process Sources, *Environmental Science & Technology*, 48, 13834-13843, 10.1021/es503696k, 2014b.

649 Li, J., Wang, Z., Zhuang, G., Luo, G., Sun, Y., and Wang, Q.: Mixing of Asian mineral dust with anthropogenic pollutants over East Asia: a model case study of a super-duststorm in March 2010, *Atmos. Chem. Phys.*, 12, 7591-7607, <https://doi.org/10.5194/acp-12-7591-2012>, 2012.

650 Li, W., Wang, C., Wang, H., Chen, J., Yuan, C., Li, T., Wang, W., Shen, H., Huang, Y., Wang, R., Wang, B., Zhang, Y., Chen, H., Chen, Y., Tang, J., Wang, X., Liu, J., Coveney, R. M., and Tao, S.: Distribution of atmospheric particulate matter (PM) in rural field, rural village and urban areas of northern China, *Environmental Pollution*, 185, 134-140, <https://doi.org/10.1016/j.envpol.2013.10.042>, 2014.

651 Li, X., Ye, C., Lu, K., Xue, C., Li, X., and Zhang, Y.: Accurately Predicting Spatiotemporal Variations of Near-Surface Nitrous Acid (HONO) Based on a Deep Learning Approach, *Environmental Science & Technology*, 58, 13035-13046, <https://doi.org/10.1021/acs.est.4c02221>, 2024a.

652 Li, Y., Qiao, L., Liu, M., Yang, Y., Yu, F., Yuan, X., Wang, Q., Ma, Q., and Zuo, J.: Access to affordable and clean domestic heating: A critical review on rural clean heating transformation in China's Jing-Jin-Ji and its surrounding areas, *Energy and Buildings*, 323, 114829, <https://doi.org/10.1016/j.enbuild.2024.114829>, 2024b.

685 Liu, J., Weng, F., and Li, Z.: Satellite-based PM2.5 estimation directly from reflectance at the top of the
686 atmosphere using a machine learning algorithm, *Atmospheric Environment*, 208, 113-122,
687 <https://doi.org/10.1016/j.atmosenv.2019.04.002>, 2019.

688 Liu, P., Zhang, C., Xue, C., Mu, Y., Liu, J., Zhang, Y., Tian, D., Ye, C., Zhang, H., and Guan, J.: The
689 contribution of residential coal combustion to atmospheric PM2.5 in northern China during winter,
690 *Atmos. Chem. Phys.*, 17, 11503-11520, 10.5194/acp-17-11503-2017, 2017.

691 Liu, R., Ma, Z., Gasparrini, A., de la Cruz, A., Bi, J., and Chen, K.: Integrating Augmented In Situ
692 Measurements and a Spatiotemporal Machine Learning Model To Back Extrapolate Historical Particulate
693 Matter Pollution over the United Kingdom: 1980–2019, *Environmental Science & Technology*, 57,
694 21605-21615, <https://doi.org/10.1021/acs.est.3c05424>, 2023.

695 Lundberg, S. M. and Lee, S.-I.: A unified approach to interpreting model predictions, *Proceedings of the*
696 *31st International Conference on Neural Information Processing Systems*, Long Beach, California,
697 USA2017.

698 Ma, S., Wang, N., Zhang, J., Ye, D., and Wang, L.: Ammonia chemistry and oxidation dynamics as dual
699 driving factors of PM2.5 nitrate pollution: Insights from the spatiotemporal disparities in central China,
700 *Journal of Environmental Management*, 392, 126594, <https://doi.org/10.1016/j.jenvman.2025.126594>,
701 2025.

702 Ministry of Ecology and Environment of the People's Republic of China: Ambient air quality standards,
703 <https://www.mee.gov.cn/ywgl/fgbz/bz/bzwb/dqjhjh/dqjhjlbz/201203/W020120410330232398521.pdf>,
704 last access: 22 October 2024, 2012.

705 Ministry of Ecology and Environment of the People's Republic of China: Report on the state of the
706 ecology and environment in China,
707 <http://english.mee.gov.cn/Resources/Reports/soc/SOEE2017/201808/P020180801597738742758.pdf>,
708 last access: 22 October 2024, 2017.

709 Park, S., Shin, M., Im, J., Song, C. K., Choi, M., Kim, J., Lee, S., Park, R., Kim, J., Lee, D. W., and Kim,
710 S. K.: Estimation of ground-level particulate matter concentrations through the synergistic use of satellite
711 observations and process-based models over South Korea, *Atmos. Chem. Phys.*, 19, 1097-1113,
712 <https://doi.org/10.5194/acp-19-1097-2019>, 2019.

713 Park, S., Lee, J., Im, J., Song, C.-K., Choi, M., Kim, J., Lee, S., Park, R., Kim, S.-M., Yoon, J., Lee, D.-
714 W., and Quackenbush, L. J.: Estimation of spatially continuous daytime particulate matter concentrations
715 under all sky conditions through the synergistic use of satellite-based AOD and numerical models,
716 *Science of The Total Environment*, 713, 136516, <https://doi.org/10.1016/j.scitotenv.2020.136516>, 2020.

717 Qin, K., Han, X., Li, D., Xu, J., Loyola, D., Xue, Y., Zhou, X., Li, D., Zhang, K., and Yuan, L.: Satellite-
718 based estimation of surface NO₂ concentrations over east-central China: A comparison of POMINO and
719 OMNO2d data, *Atmospheric Environment*, 224, 117322,
720 <https://doi.org/10.1016/j.atmosenv.2020.117322>, 2020.

721 Qiu, M., Zigler, C., and Selin, N. E.: Statistical and machine learning methods for evaluating trends in
722 air quality under changing meteorological conditions, *Atmos. Chem. Phys.*, 22, 10551-10566,
723 <https://doi.org/10.5194/acp-22-10551-2022>, 2022.

724 Qu, S., Liu, J., Li, B., Zhao, L., Li, X., Zhang, Z., Yuan, M., Niu, Z., and Lin, A.: Unveiling the driver
725 behind China's greening trend: urban vs. rural areas, *Environmental Research Letters*, 18, 084027,
726 10.1088/1748-9326/ace83d, 2023.

727 Rodriguez, J. D., Perez, A., and Lozano, J. A.: Sensitivity Analysis of k-Fold Cross Validation in
728 Prediction Error Estimation, *IEEE Transactions on Pattern Analysis and Machine Intelligence*, 32, 569-

729 575, <https://doi.org/10.1109/TPAMI.2009.187>, 2010.

730 Shen, G., Ru, M., Du, W., Zhu, X., Zhong, Q., Chen, Y., Shen, H., Yun, X., Meng, W., Liu, J., Cheng, H.,
731 Hu, J., Guan, D., and Tao, S.: Impacts of air pollutants from rural Chinese households under the rapid
732 residential energy transition, *Nature Communications*, 10, 3405, 10.1038/s41467-019-11453-w, 2019.

733 Shi, S., Chen, R., Wang, P., Zhang, H., Kan, H., and Meng, X.: An Ensemble Machine Learning Model
734 to Enhance Extrapolation Ability of Predicting Coarse Particulate Matter with High Resolutions in China,
735 *Environmental Science & Technology*, 58, 19325-19337, <https://doi.org/10.1021/acs.est.4c08610>, 2024.

736 Shi, Z., Song, C., Liu, B., Lu, G., Xu, J., Van Vu, T., Elliott, R. J. R., Li, W., Bloss, W. J., and Harrison,
737 R. M.: Abrupt but smaller than expected changes in surface air quality attributable to COVID-19
738 lockdowns, *Science Advances*, 7, eabd6696, 10.1126/sciadv.abd6696, 2021.

739 Sicard, P., Agathokleous, E., Anenberg, S. C., De Marco, A., Paoletti, E., and Calatayud, V.: Trends in
740 urban air pollution over the last two decades: A global perspective, *Science of The Total Environment*,
741 858, 160064, <https://doi.org/10.1016/j.scitotenv.2022.160064>, 2023.

742 Song, C., Liu, B., Cheng, K., Cole, M. A., Dai, Q., Elliott, R. J. R., and Shi, Z.: Attribution of Air Quality
743 Benefits to Clean Winter Heating Policies in China: Combining Machine Learning with Causal Inference,
744 *Environmental Science & Technology*, 57, 17707-17717, <https://doi.org/10.1021/acs.est.2c06800>, 2023.

745 Song, Z., Chen, B., and Huang, J.: Combining Himawari-8 AOD and deep forest model to obtain city-
746 level distribution of PM2.5 in China, *Environmental Pollution*, 297, 118826,
747 <https://doi.org/10.1016/j.envpol.2022.118826>, 2022a.

748 Song, Z., Zhao, L., Ye, Q., Ren, Y., Chen, R., and Chen, B.: The Reconstruction of FY-4A and FY-4B
749 Cloudless Top-of-Atmosphere Radiation and Full-Coverage Particulate Matter Products Reveals the
750 Influence of Meteorological Factors in Pollution Events, <https://doi.org/10.3390/rs16183363>, 2024.

751 Song, Z., Chen, B., Zhang, P., Guan, X., Wang, X., Ge, J., Hu, X., Zhang, X., and Wang, Y.: High temporal
752 and spatial resolution PM2.5 dataset acquisition and pollution assessment based on FY-4A TOAR data
753 and deep forest model in China, *Atmospheric Research*, 274, 106199,
754 <https://doi.org/10.1016/j.atmosres.2022.106199>, 2022b.

755 Southerland, V. A., Brauer, M., Mohegh, A., Hammer, M. S., van Donkelaar, A., Martin, R. V., Apte, J.
756 S., and Anenberg, S. C.: Global urban temporal trends in fine particulate matter (PM_{2.5}) and attributable
757 health burdens: estimates from global datasets, *The Lancet Planetary Health*, 6, e139-e146,
758 [https://doi.org/10.1016/S2542-5196\(21\)00350-8](https://doi.org/10.1016/S2542-5196(21)00350-8), 2022.

759 State Council of the People's Republic of China: Action Plan on Air Pollution Prevention and Control,
760 http://www.gov.cn/zwgk/2013-09/12/content_2486773.htm, last access: 22 October 2024, 2013.

761 State Council of the People's Republic of China: Assessment Method of Air Pollution Prevention and
762 Control Action Plan, http://www.gov.cn/zhengce/content/2014-05/27/content_8830.htm, last access:
763 22 October 2024, 2014.

764 Vu, T. V., Shi, Z., Cheng, J., Zhang, Q., He, K., Wang, S., and Harrison, R. M.: Assessing the impact of
765 clean air action on air quality trends in Beijing using a machine learning technique, *Atmos. Chem. Phys.*,
766 19, 11303-11314, <https://doi.org/10.5194/acp-19-11303-2019>, 2019.

767 Wang, B., Yuan, Q., Yang, Q., Zhu, L., Li, T., and Zhang, L.: Estimate hourly PM_{2.5} concentrations from
768 Himawari-8 TOA reflectance directly using geo-intelligent long short-term memory network,
769 *Environmental Pollution*, 271, 116327, <https://doi.org/10.1016/j.envpol.2020.116327>, 2021.

770 Wang, J., Lin, J., Liu, Y., Wu, F., Ni, R., Chen, L., Ren, F., Du, M., Li, Z., Zhang, H., and Liu, Z.: Direct
771 and indirect consumption activities drive distinct urban-rural inequalities in air pollution-related
772 mortality in China, *Science Bulletin*, 69, 544-553, <https://doi.org/10.1016/j.scib.2023.12.023>, 2024a.

773 Wang, R., Tao, S., Ciais, P., Shen, H. Z., Huang, Y., Chen, H., Shen, G. F., Wang, B., Li, W., Zhang, Y.
774 Y., Lu, Y., Zhu, D., Chen, Y. C., Liu, X. P., Wang, W. T., Wang, X. L., Liu, W. X., Li, B. G., and Piao, S.
775 L.: High-resolution mapping of combustion processes and implications for CO₂ emissions, Atmos. Chem. Phys., 13, 5189-5203, 10.5194/acp-13-5189-2013, 2013.
776

777 Wang, W., Zhao, C., Dong, C., Yu, H., Wang, Y., and Yang, X.: Is the key-treatment-in-key-areas
778 approach in air pollution control policy effective? Evidence from the action plan for air pollution
779 prevention and control in China, Science of The Total Environment, 843, 156850,
780 <https://doi.org/10.1016/j.scitotenv.2022.156850>, 2022a.

781 Wang, X., Wang, T., Xu, J., Shen, Z., Yang, Y., Chen, A., Wang, S., Liang, E., and Piao, S.: Enhanced
782 habitat loss of the Himalayan endemic flora driven by warming-forced upslope tree expansion, Nature
783 Ecology & Evolution, 6, 890-899, <https://doi.org/10.1038/s41559-022-01774-3>, 2022b.

784 Wang, Y., Hu, Y., Jiang, S., and Zhao, B.: Distinguishing urban-rural difference in Chinese population
785 exposure to ambient air pollutants, Atmospheric Environment, 334, 120704,
786 <https://doi.org/10.1016/j.atmosenv.2024.120704>, 2024b.

787 Wang, Y., Yu, H., Li, L., Li, J., Sun, J., Shi, J., and Li, J.: Long-term trend of dust event duration over
788 Northwest China, Science of The Total Environment, 951, 175819,
789 <https://doi.org/10.1016/j.scitotenv.2024.175819>, 2024c.

790 Wei, J., Huang, W., Li, Z., Xue, W., Peng, Y., Sun, L., and Cribb, M.: Estimating 1-km-resolution PM2.5
791 concentrations across China using the space-time random forest approach, Remote Sensing of
792 Environment, 231, 111221, <https://doi.org/10.1016/j.rse.2019.111221>, 2019.

793 Wei, J., Li, Z., Lyapustin, A., Sun, L., Peng, Y., Xue, W., Su, T., and Cribb, M.: Reconstructing 1-km-
794 resolution high-quality PM2.5 data records from 2000 to 2018 in China: spatiotemporal variations and
795 policy implications, Remote Sensing of Environment, 252, 112136,
796 <https://doi.org/10.1016/j.rse.2020.112136>, 2021a.

797 Wei, J., Li, Z., Pinker, R. T., Wang, J., Sun, L., Xue, W., Li, R., and Cribb, M.: Himawari-8-derived
798 diurnal variations in ground-level PM2.5 pollution across China using the fast space-time Light Gradient
799 Boosting Machine (LightGBM), Atmos. Chem. Phys., 21, 7863-7880, 10.5194/acp-21-7863-2021,
800 2021b.

801 Wei, J., Li, Z., Xue, W., Sun, L., Fan, T., Liu, L., Su, T., and Cribb, M.: The ChinaHighPM10 dataset:
802 generation, validation, and spatiotemporal variations from 2015 to 2019 across China, Environment
803 International, 146, 106290, <https://doi.org/10.1016/j.envint.2020.106290>, 2021c.

804 Wei, J., Li, Z., Lyapustin, A., Wang, J., Dubovik, O., Schwartz, J., Sun, L., Li, C., Liu, S., and Zhu, T.:
805 First close insight into global daily gapless 1 km PM2.5 pollution, variability, and health impact, Nature
806 Communications, 14, 8349, 10.1038/s41467-023-43862-3, 2023.

807 Wei, J., Li, Z., Cribb, M., Huang, W., Xue, W., Sun, L., Guo, J., Peng, Y., Li, J., Lyapustin, A., Liu, L.,
808 Wu, H., and Song, Y.: Improved 1 km resolution PM2.5 estimates across China using enhanced space-
809 time extremely randomized trees, Atmos. Chem. Phys., 20, 3273-3289, <https://doi.org/10.5194/acp-20-3273-2020>, 2020.

811 West, J. J., Cohen, A., Dentener, F., Brunekreef, B., Zhu, T., Armstrong, B., Bell, M. L., Brauer, M.,
812 Carmichael, G., Costa, D. L., Dockery, D. W., Kleeman, M., Krzyzanowski, M., Künzli, N., Liouesse, C.,
813 Lung, S.-C. C., Martin, R. V., Pöschl, U., Pope, C. A., III, Roberts, J. M., Russell, A. G., and Wiedinmyer,
814 C.: "What We Breathe Impacts Our Health: Improving Understanding of the Link between Air Pollution
815 and Health", Environmental Science & Technology, 50, 4895-4904,
816 <https://doi.org/10.1021/acs.est.5b03827>, 2016.

817 Xiao, Q., Zheng, Y., Geng, G., Chen, C., Huang, X., Che, H., Zhang, X., He, K., and Zhang, Q.:
818 Separating emission and meteorological contributions to long-term PM2.5 trends over eastern China
819 during 2000–2018, *Atmos. Chem. Phys.*, 21, 9475-9496, <https://doi.org/10.5194/acp-21-9475-2021>,
820 2021.

821 Xue, T., Liu, J., Zhang, Q., Geng, G., Zheng, Y., Tong, D., Liu, Z., Guan, D., Bo, Y., Zhu, T., He, K., and
822 Hao, J.: Rapid improvement of PM2.5 pollution and associated health benefits in China during 2013–
823 2017, *Science China Earth Sciences*, 62, 1847-1856, <https://doi.org/10.1007/s11430-018-9348-2>, 2019.

824 Yang, J., Lin, Z., and Shi, S.: Household air pollution and attributable burden of disease in rural China:
825 A literature review and a modelling study, *Journal of Hazardous Materials*, 470, 134159,
826 <https://doi.org/10.1016/j.jhazmat.2024.134159>, 2024.

827 Yang, N., Shi, H., Tang, H., and Yang, X.: Geographical and temporal encoding for improving the
828 estimation of PM2.5 concentrations in China using end-to-end gradient boosting, *Remote Sensing of
829 Environment*, 269, 112828, <https://doi.org/10.1016/j.rse.2021.112828>, 2022.

830 Yang, Q., Kim, J., Cho, Y., Lee, W.-J., Lee, D.-W., Yuan, Q., Wang, F., Zhou, C., Zhang, X., Xiao, X.,
831 Guo, M., Guo, Y., Carmichael, G. R., and Gao, M.: A synchronized estimation of hourly surface
832 concentrations of six criteria air pollutants with GEMS data, *npj Climate and Atmospheric Science*, 6,
833 94, <https://doi.org/10.1038/s41612-023-00407-1>, 2023.

834 Yin, J., Mao, F., Zang, L., Chen, J., Lu, X., and Hong, J.: Retrieving PM2.5 with high spatio-temporal
835 coverage by TOA reflectance of Himawari-8, *Atmospheric Pollution Research*, 12, 14-20,
836 <https://doi.org/10.1016/j.apr.2021.02.007>, 2021.

837 Yin, P., Brauer, M., Cohen, A. J., Wang, H., Li, J., Burnett, R. T., Stanaway, J. D., Causey, K., Larson, S.,
838 Godwin, W., Frostad, J., Marks, A., Wang, L., Zhou, M., and Murray, C. J. L.: The effect of air pollution
839 on deaths, disease burden, and life expectancy across China and its provinces, 1990–2017: an analysis
840 for the Global Burden of Disease Study 2017, *The Lancet Planetary Health*, 4, e386-e398,
841 [https://doi.org/10.1016/S2542-5196\(20\)30161-3](https://doi.org/10.1016/S2542-5196(20)30161-3), 2020.

842 Yu, Y., Dai, C., Wei, Y., Ren, H., and Zhou, J.: Air pollution prevention and control action plan
843 substantially reduced PM2.5 concentration in China, *Energy Economics*, 113, 106206,
844 <https://doi.org/10.1016/j.eneco.2022.106206>, 2022.

845 Yun, X., Shen, G., Shen, H., Meng, W., Chen, Y., Xu, H., Ren, Y., Zhong, Q., Du, W., Ma, J., Cheng, H.,
846 Wang, X., Liu, J., Wang, X., Li, B., Hu, J., Wan, Y., and Tao, S.: Residential solid fuel emissions
847 contribute significantly to air pollution and associated health impacts in China, *Science Advances*, 6,
848 eaba7621, 10.1126/sciadv.eaba7621, 2020.

849 Zhai, S., Jacob, D. J., Wang, X., Shen, L., Li, K., Zhang, Y., Gui, K., Zhao, T., and Liao, H.: Fine
850 particulate matter (PM2.5) trends in China, 2013–2018: separating contributions from anthropogenic
851 emissions and meteorology, *Atmos. Chem. Phys.*, 19, 11031-11041, <https://doi.org/10.5194/acp-19-11031-2019>, 2019.

853 Zhang, H., Di, B., Liu, D., Li, J., and Zhan, Y.: Spatiotemporal distributions of ambient SO₂ across China
854 based on satellite retrievals and ground observations: Substantial decrease in human exposure during
855 2013–2016, *Environmental Research*, 179, 108795, <https://doi.org/10.1016/j.envres.2019.108795>, 2019a.

856 Zhang, Q., He, K., and Huo, H.: Cleaning China's air, *Nature*, 484, 161-162,
857 <https://doi.org/10.1038/484161a>, 2012.

858 Zhang, Q., Shi, R., Singh, V. P., Xu, C.-Y., Yu, H., Fan, K., and Wu, Z.: Droughts across China: Drought
859 factors, prediction and impacts, *Science of The Total Environment*, 803, 150018,
860 <https://doi.org/10.1016/j.scitotenv.2021.150018>, 2022a.

861 Zhang, Q., Zheng, Y., Tong, D., Shao, M., Wang, S., Zhang, Y., Xu, X., Wang, J., He, H., Liu, W., Ding,
862 Y., Lei, Y., Li, J., Wang, Z., Zhang, X., Wang, Y., Cheng, J., Liu, Y., Shi, Q., Yan, L., Geng, G., Hong, C.,
863 Li, M., Liu, F., Zheng, B., Cao, J., Ding, A., Gao, J., Fu, Q., Huo, J., Liu, B., Liu, Z., Yang, F., He, K.,
864 and Hao, J.: Drivers of improved PM2.5 air quality in China from 2013 to 2017, Proceedings of the
865 National Academy of Sciences, 116, 24463-24469, <https://doi.org/10.1073/pnas.1907956116>, 2019b.
866 Zhang, X., Brandt, M., Tong, X., Ciais, P., Yue, Y., Xiao, X., Zhang, W., Wang, K., and Fensholt, R.: A
867 large but transient carbon sink from urbanization and rural depopulation in China, *Nature Sustainability*,
868 5, 321-328, <https://doi.org/10.1038/s41893-021-00843-y>, 2022b.
869 Zhao, B., Zheng, H., Wang, S., Smith, K. R., Lu, X., Aunan, K., Gu, Y., Wang, Y., Ding, D., Xing, J., Fu,
870 X., Yang, X., Liou, K.-N., and Hao, J.: Change in household fuels dominates the decrease in PM2.5
871 exposure and premature mortality in China in 2005–2015, *Proceedings of the National Academy of
872 Sciences*, 115, 12401-12406, <https://doi.org/10.1073/pnas.1812955115>, 2018.
873 Zheng, B., Tong, D., Li, M., Liu, F., Hong, C., Geng, G., Li, H., Li, X., Peng, L., Qi, J., Yan, L., Zhang,
874 Y., Zhao, H., Zheng, Y., He, K., and Zhang, Q.: Trends in China's anthropogenic emissions since 2010 as
875 the consequence of clean air actions, *Atmos. Chem. Phys.*, 18, 14095-14111, <https://doi.org/10.5194/acp-18-14095-2018>, 2018.
876 Zheng, H., Kong, S., He, Y., Song, C., Cheng, Y., Yao, L., Chen, N., and Zhu, B.: Enhanced ozone
877 pollution in the summer of 2022 in China: The roles of meteorology and emission variations,
878 *Atmospheric Environment*, 301, 119701, <https://doi.org/10.1016/j.atmosenv.2023.119701>, 2023.
879 Zhong, Q., Ma, J., Shen, G., Shen, H., Zhu, X., Yun, X., Meng, W., Cheng, H., Liu, J., Li, B., Wang, X.,
880 Zeng, E. Y., Guan, D., and Tao, S.: Distinguishing Emission-Associated Ambient Air PM2.5
881 Concentrations and Meteorological Factor-Induced Fluctuations, *Environmental Science & Technology*,
882 52, 10416-10425, <https://doi.org/10.1021/acs.est.8b02685>, 2018.
883 Zhong, Q., Tao, S., Ma, J., Liu, J., Shen, H., Shen, G., Guan, D., Yun, X., Meng, W., Yu, X., Cheng, H.,
884 Zhu, D., Wan, Y., and Hu, J.: PM2.5 reductions in Chinese cities from 2013 to 2019 remain significant
885 despite the inflating effects of meteorological conditions, *One Earth*, 4, 448-458,
886 <https://doi.org/10.1016/j.oneear.2021.02.003>, 2021.
887

888